Laser Induced Electron Photodetachment in a Flowing Afterglow

by

Edward John Bianchina, Jr.

B.S., Northwest Missouri State University, 1986

A MASTER'S THESIS

submitted in partial fulfillment of the

requirements for the degree

MASTER OF SCIENCE

Department of Chemistry

KANSAS STATE UNIVERSITY

Manhattan, Kansas

1989

Approved by:

Major Professor

Table of Contents

List of Tables.

List of Figures.

I. Laser Induced Electron Photodetachment in a Flowing Afterglow.

I.A. Background for the Photochemistry of Molecular Anions.

The determination of the electron affinities of neutral species is of great importance in several areas[1] that range from analytical mass spectroscopy[2] to toxicity of biological compounds.[3] A recent review describes a number of recent advances in the field.[4] Several methods for determining the electron affinities (EA) of atoms, diatomics, and polyatomic neutrals have been used in the past and are currently in use. These include charge bracketing, high pressure mass spectrometry,[5] photoelectron spectroscopy (PES),[6] and ion cyclotron resonance electron photodetachment (ICREPD).[7] This section will present a survey of these methods along with the advantages and disadvantages of each method.

The electron affinity of a neutral species is the energy changed when an electron is added to a neutral molecule to form the corrisponding negative ion as shown in eq. 1. In this equation the thermochemical change is the adiabatic EA, EA(A), of the neutral with a

$$A + e^- \longrightarrow A^- \; ; \; \Delta H_0^0 = -EA \qquad (1)$$

change in sign. The EA is also the ionization potential of the anion. The ion and the neutral must be in their ground rotational, vibrational, and electronic states, for the adiabatic EA. This is represented by the potential energy curves for the anion in relation to the neutral species plus the electron shown in Figure 1. The lower curve represents the anion A^- and the upper curve is the neutral.

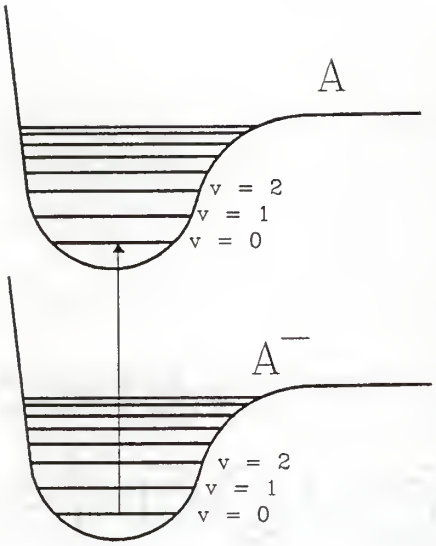

Figure 1. Potential energy curves for an adiabatic EA.

There may be geometry changes between A^- and A, since bond distances and bond angles may be different. However, the adiabatic EA only involves the difference between the ground state of A and the ground state of A^-. The vertical and adiabatic EAs in the process shown in Figure 1 are the same. If A^- and A have different geometries, the adiabatic and vertical EAs differ (Figure 2). In addition to the energy requirements for the molecular moiety the electron should possess no energy when it leaves the molecule.

I.A.1. Charge Transfer Bracketing.

The most precise method of EA determination is by chemical reaction techniques. In this technique the EA of the species A is bracketed between the known EAs of other molecules. There are three methods

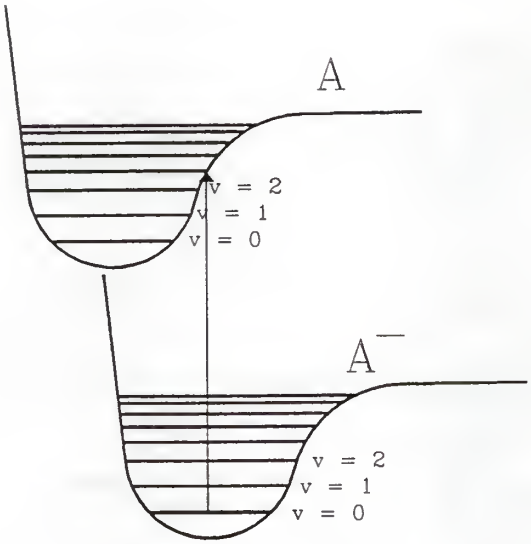

Figure 2. Potential energy curves for a nonadiabatic EA.

used, electron transfer equilibria[8], and endothermic[9,10] and exothermic charge transfer.[11] These kinetic methods take advantage of the known ΔH_f^o of species to determine the EA of the species of interest. Equations 2a and 2b illustrate both process. Equation 2a can be utilized in both the exothermic and endothermic cases while eq

$$A^- + B \rightarrow A + B^- \qquad (2a)$$

$$A + B \rightarrow A^+ + B^- \qquad (2b)$$

2b is strictly used in the endothermic technique.

For endothermic charge transfer reaction, an ion beam is accelerated to a known average translational energy and filtered according to these velocities. The beam of ions with known velocity are allowed tc collide with a neutral B molecule. The ion is given

only enough energy to produce a reaction. The EA(A) is then the translational energy of this ion minus the EA(B).

The exothermic charge transfer reaction requires that the overall process is exothermic. If the reaction between A^- and B produces A and B^-, EA(B) > EA(A). This method requires that A^- is reacted with a series of different neutral molecules of known EAs. The reactions are continued until electron transfer is no longer observed. These results bracket EA(A) between the lowest EA of the neutrals which underwent charge transfer and the largest EA of the neutrals which did not.

An example of this approach is represented by the rough determination of EA($\underline{c}$-C_5H_4).[12] In this case the corresponding carbene anion radical, $\underline{c}$-$C_5H_4^{\bullet -}$, reacted slowly with C_6F_6 to produce aromatic substitution, but no charge transfer product. This means that EA($\underline{c}$-C_5H_4) $\geq$ EA(C_6F_6) $\geq$ 12.0 $\pm$ 7 kcal mol^{-1}.[13] The upper limit of the EA($\underline{c}$-C_5H_4) was established by the reaction of $\underline{c}$-$C_5H_4^{\bullet -}$ with NO_2 which formed NO_2^- as one of the product ions. Thus, (12.0 $\pm$ 7 kcal mol^{-1}) = EA(C_6F_6) $\leq$ EA($\underline{c}$-C_5H_4) $\leq$ EA(NO_2) $\leq$ (54.4 $\pm$ 2 kcal mol^{-1}).[14]

This method relies upon the predetermined values of the bracketing reagents, which are sometimes inaccurately known and the uncertainties associated with this technique can be large.

High pressure mass spectrometry (HPMS),[5] as well as ion cyclotron resonace (ICR) spectroscopy, use electron transfer equilibria to measure the EA's of a large number of compounds.[15] In these methods, the equilibrium constant for a reaction of the type in eq. 3a is determined. HPMS generates ions at a pressure of 5 torr by electron attachment to suitable neutral precursors. The high pressure mixture

of buffer gas, A^- and B^- are monitored by mass spectrometry with a known amount of added B. These componants react to yield an equilibrium mixture. Once this equilibrium has been reached, the ratio of concentration of the two ions is constant and the equilibrium constant can be calculated. From the equilibrium constant, K, ΔG°_T of the equilibrium in eq. 3a can be calculated by eq. 3c.[5] The EA(A) can be defined as the heat of reaction between e^- and B or the heat of attachment (ΔH°_a) of an electron to B. In the same sense the ΔG° of the attachment process is defined as ΔG°_a. The equilibrium in eq. 3a represents the difference between the EAs of A and B.

$$A^- + B = A + B^- \tag{3a}$$

$$K = \frac{[A][B^-]}{[A^-][B]} \tag{3b}$$

$$\Delta G_{3a}{}^\circ = -(RT)\ln K_{3a} = \Delta H_{3a}{}^\circ - T\Delta S_{3a}{}^\circ \tag{3c}$$

$$\Delta H_{3a}{}^\circ = \Delta H_a{}^\circ(B) - \Delta H_a{}^\circ(A) \tag{3d}$$

$$-EA(B) \approx \Delta H_a{}^\circ(B) \tag{3e}$$

The ΔS°_{3a} is derived from a van't Hoff plot of K_{3a} vs. temperature or estimated. A series of interconnected ΔG° or ΔH° values are calculated and then the EA's are "anchored" with a known value for one of the species in the series. This method must be cautiously used due the heavy dependence of all values of EA's depends upon the EA anchors. This approach caused problems in the past due to an incorrect assignment of the anchor EA values.[8a] Several examples of this method are presented in a recent review.[5]

I.A.2. Photoelectron Spectroscopy.

Photoelectron spectroscopy (PES) has proven to be a versatile method[16,17] for determining a number of EA's as well as the spectroscopy[18] of reactive species.[19] Negative ions produced from a source are extracted and mass selected. The ion source may involve electron impact, a microwave or hollow cathode discharge at low pressures or relatively high pressure of a flowing afterglow.[18] The mass selected ion beam is directed into the ion/light interaction region where the ion beam is crossed at right angles with the output of a laser. Electrons are detached at the intersection of the two beams and energy analyzed. Only those photoelectrons that are detached at 90° from the ion and laser beam intersection plane are analyzed. The photoelectrons translational energy will be due only to the detachment process. The resulting photoelectrons enter a hemispherical electron energy analyzer which counts the number of electrons as a function of their energy which yields the PES spectrum.

Calibration factors must be determined for accurate measurements. Because of various contact potentials, which are slight voltage differences between various pieces of the apparatus, the true energy of the electrons is shifted from the measured values. To solve this problem, a species whose photoelectron spectrum is known is run either before or after as a standard for comparison. Typically, O^- or OH^- is used for this purpose due to several sharp transitions in these negative ions.

A reference frame problem associated with the detached photoelectrons must also be solved. Since the energy analyzer is in

the lab frame of reference and the ions are in the center-of-mass (C.M.) reference frame, the electrons that are ejected are, in fact, slightly back scattered relative to the C.M. frame. This will shift the apparent electron energy from the true value, due to the additional translational energy of these photoelectrons.

The energy scale can also be compressed or expanded due to deviations from the true 90° detection angle. Another standard is used to correct this problem. NH^- is used because it contains two electronic transitions whose splitting is known from optical spectroscopy.[20] This splitting, 1.562 eV, is wide enough to be used as an index of compression or expansion of the energy scale.

The last problem to solve is the energy analyzer transmission function, which is the efficiency of the analyzer as a function of electron energy. This presents a problem only if the relative intensities of PES peaks need to be known. The use of O_2^- as a standard is utilized. The ion optics can be tuned to flatten the transmission curve of the analyzer. The spectrum of O_2^- is repeatedly taken and the optics are adjusted to give the spectrum with known intensities.[21]

To determine both the EA of the neutral and the spectroscopy of the anion and/or the resulting neutral, each vibrational transition in a long series of these transitions must be assigned. This must be done to identify the T_o transition. This can be difficult, as illistrated by the history of a small molecule such as CH_2^-. Because CH_2 is the simplest carbene, its structure, energies, and spectroscopy have been

extensively studied.[22] The ground state of methylene is $^3B_1$ with a H-C-H angle of 132°. The lowest excited state, $^1A_1$, has been calculated to be 10 kcal mol^{-1} above that of that ground state.[23] Kinetic[24] as well as heat of formation differences[25] agree with calculated values and give the singlet-triplet splitting near 8 kcal mol^{-1}. Lineberger, et al.[26] first measured the singlet-triplet splitting by PES in 1976. as 19.5 ± 0.7 kcal mol^{-1}. This is well outside the values of previous results. The discrepancy between previous values for the splitting and Linebergers results were the incorrect assignment of the 0 ← 0 transition. This was due to vibrationally excited species present in the first reported results and to the difficulty of spectral assignments because of the bending angle of CH_2 and CH_2^- differ. These first experiments were conducted in an apparatus that did not allow the generated ions to be cooled to their ground vibrational states. Since the first report, the photoelectron spectrometer was modified to use a flowing afterglow as the negative ion source.[18a] With this source the correct splitting was determined to be 8.98 kcal mol^{-1}, which agrees with previous calculations.

In addition to the incorrect singlet-triplet splitting assignment, the EA of the ground state of CH_2 was also in error. The preliminary report of EA(CH_2($^3B_1$)) = 0.210 ± 0.03 eV (4.841 kcal mol^{-1}) was corrected in the more recent paper to be 0.645 ± 0.006 eV (14.87 kcal mol^{-1}).[18]

I.A.3. Electron Photodetachment.

I.A.3.a. Ion Cyclotron Resonance.

Ion cyclotron resonance (ICR) spectroscopy is another useful method for the generation and study of the photochemistry of negative ions.[27,28] Basically, the ICR consists of a trapped ion cell in a metal vacuum can held between the poles of an electromagnet or superconducting magnet. Potentials are placed on the sides of the metal cell to trap the ions generated by electron impact or ion/molecule reactions in the cell. The ions so generated in a strong magnetic field travel in their cylotron orbits. Because the pressures are low (10^{-8} torr),[27a] the ions may be trapped for up to several seconds. Ions are detected by having two of the sides of the cell in a marginal oscillator circuit and bringing the ions into resonance by changing the driving radio frequency. By fixing the radio frequency, only the ions not in resonance with the rf frequency are retained in the cell while the other ions absorb the rf energy which increases their cyclotron orbits untill they are lost to the walls.

To determine the electron photodetachment (EPD) spectrum, the ions are allowed to interact with light. At one end of the vacuum can is a window through which the photons enter the vacuum can and the trapped ion cell. The light source can be either a 1000 W xenon arc lamp or the output from a tunable dye laser. A monochromator is used to increase the resolution when the arc lamp is used as the light source. This experiment has a full-width-half-maximum (FWHM) resoultion of approximatly 23 to 40 nm while the dye laser has a FWHM of less than an angstrum. A mirror is placed at the back of the cell to increase the EPD by reflecting the light back through the cell. The light intensity from the monochromator is measured by a thermopile following each run.

The power of the dye laser is measured by splitting the beam and directing a small portion of the light onto a thermopile.

Several disadvantages do exist with the ICREPD experiment. A major concern is that the negative ions may not be in the ground vibrational, and rotational states because the low pressure in which the ions are generated. Since the electron impact and the ion/molecule reactions are exothermic processes, the ions carry away much of this excess energy. Because the ions will undergo a limited number of collisions with thermal molecules, the EPD may come from an excited species and not from the ground state of the ion. Since the distribution of these excited states cannot be determined, the identification of vibrational transitions is difficult.

I.A.3.b. Drift Tube

One of the most versatile methods used for studies of the interaction of light and ions utilize a drift tube apparatus.[29] The sequential layout of the instrument is an ion source, a drift tube, and an ion detection region. In this apparatus the electrons are produced by an electron gun with controlled energy in the flow of a buffer gas. The ions are formed by electron impact on neutral precursors upstream of the drift region. The ions are extracted[29a] into the drift region and the rate at which they move down the flow tube is controlled by a weak, uniform electric field towards an 1 mm extraction aperture. The ions are extracted from the high pressure drift region (0.05 torr to 1.0 torr) into a low pressure mass analysis region (10^{-5} torr) containing a quadrupole mass spectrometer where the

ions are mass analyzed and counted. The typical count rates are 10^3 to 10^5 ions sec^{-1}. Before exiting the drift region, the ions must pass through a laser beam that passes directly in front of the extraction aperture. The laser beam is chopped and the ions are counted with laser-on and laser-off cycles so that the differences between laser-on and laser-off can be determined.

The photon source in these experiments must be intense, due to the short time the ion spends in the light beam (typically 10^{-5} sec), and tunable over a wide range of energies. To achieve a high photon flux a laser system must be used. By extending the cavity of an argon ion laser to include a cross section of the drift region, Moseley and co-workers[29a] were able to generate radiation sufficently intense to observe EPD and photodissociation (PD) of negative ions[29] and photodissociation (PD) of positive ions.[29] This allowed for the measurement of cross sections at seven discrete wavelengths of an argon ion laser. This course spectrum presents problems with identifying thresholds or any rotational or vibrational fine structure associated with the process.

To overcome this problem, the photon energy must be continuously tunable. This was accomplished by employing an argon ion laser to pump a tunable dye laser.[29j] The optics of the dye laser (minus the standard output coupler) became one end of the extended cavity, which includes the cross section of the drift region. The circulating photon power is as high as 220 watts (although the values ranged from 13 watts to 220 watts).[30] This allows for the detection of small ($\leq$ 0.5%) ion losses to be measured. Mosely, et al.[33a] then calibrated the

instrument for exact cross sections to be determined by determining the cross sections for O_2^- at various wavelengths, which are known.

One of the ions studied was the PD of CO_3^- .[33g] The goal of this study was to determine the photochemistry of this negative ion, which is formed by the ion/molecule reaction of O^- and CO_2. By varying the drift distance and, in turn, the number of cooling collisions the ion had with the buffer gas, the lowest vibrational state of the ion was obtained. This determination was made from the fact as the degree of vibrational excitation (vibrational population) changed, the relative intensities of the PD peaks also changed. This would hold true except for one peak, the ground state of the anion. The intensity of the transition from the ground state of the anion to the ground state of the corresponding neutral would not be effected by the relative populations in the upper states. Indeed, the experiment showed that the intensity of the peak at 1.85 eV was not effected by the degree of vibrational excitation, while a peak at 2.41 eV was dependent upon the excess vibrational energy. The peak at 1.85 eV was then assigned as detachment from the vibrational ground state.

Because PD is from the equilibrium ground state of the anion to an unknown state of the neutral species, the PD can only be an upper boundary on the bond dissociation energy, $D°(CO_2\text{-}O^-)$. A upper limit for $D°(CO_2\text{-}O^-)$ had been reported from an equilibrium constant measurement and was 2.0 ± 0.2 eV.[31] Since PD occurred at 1.8 eV, the 1.8 eV ≤ $D°(CO_2\text{-}O^-)$ ≤ 2.0 eV. From the relationship given in eq 4, the electron affinity

$$EA(CO_3) = D°(CO_2\text{-}O^-) + EA(O) - D°(CO_2\text{-}O) = 2.9 \pm 0.3 \text{ eV} \qquad (4)$$

can be calculated. The values used were $D°(CO_2\text{-}O^-)$ = 1.8 eV, EA(O) = 1.462 eV,[32] and $D°(CO_2\text{-}O)$ = 0.4 ± 0.2 eV.[33a] The value was calculated to be $EA(CO_3)$ = 2.9 ± 0.3 eV. Hong, Woo, Helmy[33] determined $EA(CO_3)$ = 2.69 eV by drift tube methods, which is consistent with the value in eq 4.

I.B. Objective of This Research.

The objective of this investigation is to develop a method for the accurate measurement of the thresholds for electron photodetachment (EPD) of ground state organic negative ions generated in a flowing afterglow (FA) apparatus. The resolution and accuracy of the laser/FA system will be determined by measuring the EPD spectra of two organic negative ions, acetophenone enolate anion ($C_6H_5C(O^-)=CH_2$) and cyclopentadienyl anion ($\underline{c}$-$C_5H_5^-$), in the threshold region. The EPD spectrum of $C_6H_5C(O^-)=CH_2$, produced in an ion cyclotron resonance spectrometer (ICR), and the EPD threshold of $\underline{c}$-$C_5H_5^-$, determined by photoelectron spectroscopy (PES), have been reported. After confirming the reliability of the system the EPD threshold for cyclopentadienylidene anion radical ($\underline{c}$-$C_5H_4^{\bullet -}$) was found to be 40.36 ± .007 kcal mol^{-1}.

I.C. Experimental

I.C.1. The Flowing Afterglow Apparatus.

The measurement of the electron photodetachment (EPD) spectra was carried out in a flowing afterglow (FA) apparatus (Figure 3). The FA can be divided into three functionally different regions: ion production and ion reaction regions, and a differentially pumped

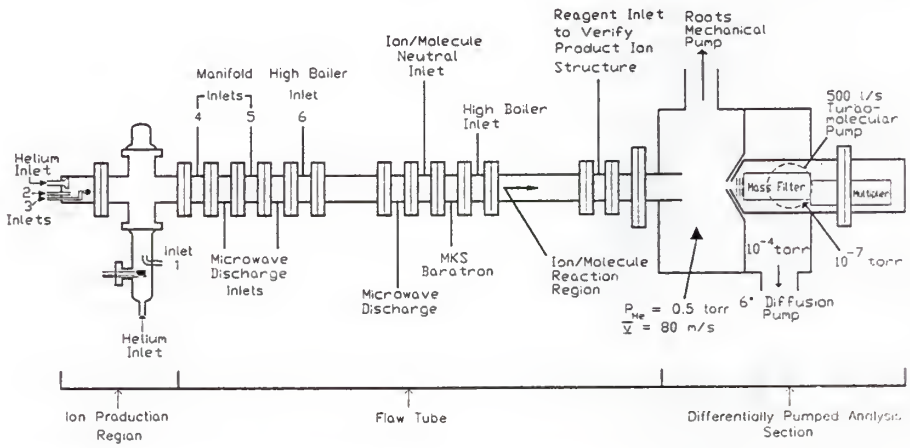

Figure 3. The flowing afterglow (FA) apparatus.

region, which contains the quadrupole mass filter and electron multiplier. Each region provides a specific purpose that will be discussed.

I.C.1.a. General Considerations.

In general, a flow of helium buffer gas is added at the upstream end of the flow tube. Approximately 80% of the helium is added via the upstream inlet with the remainder being added via the inlet at the bottom of the Pyrex glass side-arm containing the electron gun. The

constant flow of helium is maintained by a large, fast pumping system, and is controlled by a throttling gate valve. By adjusting this gate valve, the flow tube pressure and helium gas velocity can be varied from P_{He} = 0.3 to 1.4 torr and $\underline{v}$ = 100 to 25 m/s. While the major part of the gas flow is removed by the large, fast pumping system, the flow is sampled via 1 mm orifices in each of two molybdenum nose cones into the differentially pumped compartments containing the quadrupole mass filter and electron multiplier detector.

The ions are generated continuously by electron impact on small amounts of gaseous neutral precursors added via inlet 1, or by a sequence of ion/molecule reactions. The initially generated ions are collisionally stabilized with the buffer gas as the ions move down the flow tube entrained in the helium.

I.C.1.b. The Flow Tube.

The flow tube is a 135 cm long stainless steel pipe with an inside diameter of 7.15 cm (Esco Products, Inc.). The tube is of a modular design with individual units bolted together with O-ring seals. This allows for easy modification of the flow tube by removal and addition of modular units. The flow tube pressure and flow velocity are controlled by a combination of the added helium flow, monitored by a tri-flat flowmeter (Fisher & Porter #449-306), and throttling the gate valve that connects the FA to the Stokes roots blower/mechanical pump (Model 1722-S) via an 8 in. OD aluminum duct. The flow tube inlets are glass and annular in design with small holes punched into the inside

surface of the glass tube. This allows for the near planar mixing of gases into the laminar flow within the flow tube.

I.C.1.c. Ion Production Region.

The ion gun consists of a filament of appropriate material suspended under an accelerating grid (made from tungsten mesh). The filaments are made of either rhenium metal or thorium oxide coated iridium (Electron Technology). A current is applied to the filament held at a high negative potential while the grid is grounded. The electrons are accelerated from the filament causing ionization of the helium buffer gas and generating an ion/electron plasma. This plasma then passes through the grid. The power supply for the filament was a Hewlett Packard series MPB-S, model 6286A DC that delivers 0 to 24 volts and 0 to 12 amps. The accelerating voltage is supplied by a Keithley model 245 high voltage regulated power supply that applied a 0 to -300 volt potential between the filament and the grid. The emission current emitted was monitored by a standard ammeter (Micronta, model 22-204c) capable of monitoring < 50 microamps to > 10 milliamps.

The electron gun could be mounted either (a) directly in the flow tube or (b) in the Pyrex glass side-arm where the electron/ion plasma is generated at a 90° angle to the flow tube. Each position has certain advantages. With the electron gun in position (a), low mass ions ($m/z < 40$) are more readily observed in the downstream flow. These low mass ions, apparently, do not efficiently make the 90° turn with the electron gun located in position (b). Placement of the electron gun in the Pyrex glass side-arm (position (b) shown in Figure

3) is used for the ion/molecule reaction studies where high emission currents are necessary for specific transition-metal complex negative ion generation. Since time-sharing on the FA used in this study involved several members of the group, the side-arm was used in the present studies.

An example of ion production is illustrated by generation of c-$C_5H_4^{\bullet -}$. The precursor diazo compound, c-$C_5H_4N_2$, is leaked into the flow tube via inlet 1 where it undergoes dissociative electron attachment (DEA). This cleavage is possible because the electron affinity (EA) of c-$C_5H_4N_2$ is greater than the bond dissociation energy (D°) of the carbon-nitrogen bond. The fragment negative ion undergoes collisional stabilization with the helium buffer gas, which removes the excess vibrational energy from the initially formed excited negative ion. The ion relaxes to a Boltzman vibrational distribution.

Alternatively, the ions of interest may be generated by using one or more ion-molecule reactions to provide the needed ions. For example, to generate acetophenone enolate anion, a small amount of NF_3 is added via inlet 1, undergoes DEA to produce F^-. Acetophenone which is added at either inlets 2, 3, 4 or 5 which undergoes H^+ transfer with F^- to yield HF and acetophenone enolate anion. By using these two methods, a large number of ions can be generated.

I.C.1.d. Differentially Pumped Region.

Since the ion generation and the ion/molecule reactions are carried out in the flow tube at a relatively high pressure (P_{He} = 0.5 to 1.2 torr) and the mass analysis of the ion flow must be carried out

at low pressures ($P_{He} < 10^{-6}$ torr), differential pumping is used to mate the pressure extremes. As shown in Figure 3, the box connected to the downstream end of the flow tube consists of three compartments, which are pumped separately and interconnected by 1 mm orifices in each of two molybdenum nose cones. The majority of the main gas flow is removed by the Stokes roots blower/mechanical pump from the first compartment of the box. However, the main gas flow is sampled via the first nose cone orifice into the second compartment of the box, which is pumped a by Varian 6" oil diffusion pump backed by a Sargent-Welch mechanical pump (model 1397) to a pressure of ca. 10^{-4} torr. This gas/ion mixture is further sampled via the second nose cone 1 mm orifice into the vacuum can containing the quadrupole mass filter and electron multiplier, which is pumped by a Phieffer THP-500 turbomolecular pump backed by Sargent-Welch mechanic pump (model 1376) which maintains a pressure of $<5 \times 10^{-6}$ torr when the flow reactor is in use.

The first molybdenum nose cone and its aluminum holder are electrically isolated from each other, and the nose cone holder is isolated from the stainless steel main housing with teflon and plastic spacers. The second nose cone is also electrically isolated from the main housing with a small plastic spacer. Electrical feed-throughs are connected to both nose cones and the the first nose cone holder so that DC potentials of 0 to ± 24 volts can be placed on these components to aid the ion sampling.

The ions that pass through the second nose cone encounter a set of six ion lenses that focus and select the correct energy of the ions

before they pass into the quadrupole mass filter region; typical nose cone and lens potentials are given in Table I. The quadrupole mass filter is made up of four stainless steel rods in a square-box arrangement with the ions passing down the length of the rods. An RF potential is placed on two opposite rods and a DC potential is placed

Table I. Lens Settings and Nose Cone Potentials for Negative Ion Detection.

Lens	Potential
1	+80.8 mV
2	+21.4 mV
3	+60.2 mV
4	+ 9.6 mV
5	+88.7 mV
6	+23.3 mV
Nose Cone 1	- 2.0 V
Nose Cone Holder	-24.0 V
Nose Cone 2	+24.0 V

on the other two opposite rods. The RF potential is of the correct frequency so that only the ions with the correct mass for the applied field are allowed to pass cleanly through to the analysis section. All other ions are ejected. If the RF frequency is scanned, the mass of the ions allowed to pass through the quadrupole mass filter is also scanned and the mass spectrum is obtained. The resolution is defined as the accuracy with which the the quadrupole mass filter obtains the

total separation of different mass ions. The experiment starts by scanning the RF potential. In this manner the composition of the flow can be determined. This can be done on moderate resolution (total separation of ions whose masses differ by 2 to 3 amu).

For the EPD study the quadrupole was operated in the single ion mode. In this mode, the RF and DC potentials are held constant so that an ion of selected mass is continuously monitored (generally with low resolution). The instrument is set (by the resolution and ΔM controls) to be less selective in terms of ion energies allowed into the quadrupole region. This allows for larger ion signals yielding better signal-to-noise ratio in the EPD experiments. Typically the resolution was set so that the base of the "single" ion mass spectrum peak covered 2 to 5 amu.

The ion lenses, mass filter, and electron multiplier are components of an Extrel C-50 quadrupole mass spectrometer. The C-50 employs a conversion dynode, which converts the mass selected negative ions into positive ions for detection and counting. Negative ions are attracted to a metal plate of the conversion dynode which is held at a +4kV potential. The major processes, which occur from the impact, are charge stripping of the negative ion and sputtering of the metal surface, both of which yield positively charged ions. These positive ions are attracted to the opening of the Channeltron electron multiplier held at a -2 kV potential. The impact of positive ions with the surface of the multiplier ejects several electrons. Each of these electrons will strike the multiplier surface again to eject more electrons. This leads to the 10^6 gain for the multiplier.

I.C.2. Laser and Data Acquisitions Systems.

The schematic diagram of the equipment showing the FA, the lasers, and associated apparatus is shown in Figure 4. A Coherent 20 watt INNOVA 100 argon ion laser operated in the multiline visible mode was

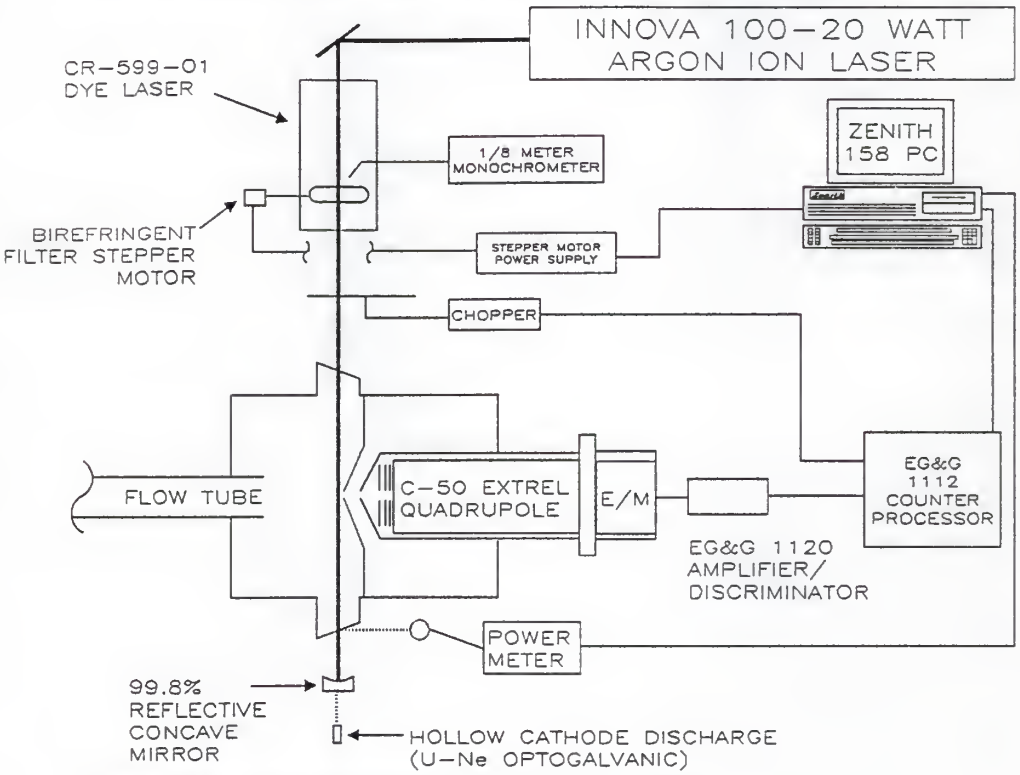

Figure 4. Laser and data acquisition system.

used to optically pump a solution of organic dyes pumped through a modified Coherent CR-99-01 dye laser. The dyes used were Rhodamine 110, Rhodamine 6G, and DCM. The modification of the laser was necessary because the output from a stock cavity of the laser would not allow for the observance of photodetachment due to low laser power. The cavity of the dye laser was extended from the normal 50 cm to about

1.5 meters to include a cross section of the FA within the extended cavity.[34, 33a] This was accomplished by removing the dye laser's flat output coupler (reflectively of about 96%) and placing a concave mirror (reflectively > 99.8%, radius of curvature 1.5 meters; CVI Laser Corp.) on the far side of the FA main housing. The dye laser head and the high reflective mirror were placed so that the cavity photon beam passed directly in front of the FA's first sampling nose cone orifice. This means the ions that were to be mass analyzed and counted passed through this beam.

The radius of curvature of the extended cavity high reflective mirror made the focal point of the mirror approximately in the middle of the extended cavity.[38] In the standard short cavity operation of the dye laser, the beam is focused 20 to 30 cm from the high reflective output coupler, which was also approximately the middle of the extended cavity. With the extended cavity output coupler focused at 75 cm from its surface, the two focal points coincide. This focal point allowed a photon to travel between the laser cavity mirrors on the same path and allows for lasing. The differentially pumped box of the FA was fitted with two quartz windows oriented at Brewsters angle to allow the beam to pass through the box with low loss of power due to reflection from these windows.

The laser system stood on a 4' x 8' Newport optical table. The table and standard fixed mount table legs were placed on 6" x 7" x 9.5" solid aluminum blocks to bring the table to the correct height to allow the photon beam to pass though the windows and in front of the nose cone orifice in the FA. The far side high reflector was housed in a

Newport mirror mount (Model 600A2), bolted to a 4" x 6" x 3" aluminum block which was placed upon a stack of four 8" cinder blocks separated by 1/4" thick firm rubber pads. Both the blocks and the mirror mount were separated from the FA support table and pumps to avoid vibrations.

Just before the ions entered the orifice of the first nose cone they passed through the laser beam. If the wavelength of the light was correct, a percentage of the negative ions would detach an electron. The difference between the number of ions entering the mass analysis section with the laser on, as compared to the number of ions entering with laser off, was related to the cross-section at that wavelength. To obtain laser-off and laser-on signals, a light chopper (EG&G, Model 196) was placed just in front of the dye laser; the chopping frequency was 100 Hz. The chopper was then connected to its control unit which was connected to a photon counter/processor (EG&G Model 1112). As mentioned previously, the mass spectrometer was operated in the single ion mode. The analog signal from the mass spectrometer was fed into an amplifier/discriminator (EG&G Model 1120) that had been adjusted for the correct count threshold level.

The digital TTL pulse signal from the amplifier/dicriminator is fed into the photon counter/processor which was located. The average of ions counted and used in cross-section calculation (with the chopper open (laser-on) and closed (laser-off)) was an average of individual samples (usually 10 to 30 samples/average) taken from the photon counter. Each of these individual samples consisted of 100 to 1000 counting cycles. These counting cycles were for a predetermined period (35 μs at 100 Hz chop frequency) during the chopper cycle with the

laser on and off when the photon counter counted the individual ion events detected by the electron multiplier. The counting cycle was timed from the reference signal of the chopper. The chopper cycle must be calibrated so that when the chopper blade blocks the photon beam, the photon counter/processor stops that counting cycle. If the chopper is misaligned, the photon counter/processor will detect a small amount of the background counts into the data counts and a small amount of the data counts into the background counts. This will, in effect, decrease the amount of percent detachment and will lower the EPD spectrum. At large fractional detachments, the EPD spectrum will look normal, but for small fractional detachments the EPD spectrum will prematurely fall to zero. The alignment was accomplished by sighting the timing of the photon beam blockage with the counting cycle indicators on the photon counter/processor. Two sets of numbers were output from the photon counter/processor each time, one for the laser-off (background) and one for the laser-on data. A homemade circuit designed and built by John Linzi was used to transfer this data to an Zenith Z-158 PC. The homemade circuit is necessary because the output from the factory equipped photon counter allowed for only three significant digits to be transferred to the computer. Since the number of counts was $> 1 \times 10^5$, the lowest percent detachment able to be seen by the 3 significant digits was 1%. For accurate data, percent detachments of $< 0.1\%$ were needed. The design of the photon counter was such that eight digits of data were counted into data registers then transferred to display and output buffers of the instrument. It was in the display and output buffers that the loss of the lowest five significant digits occurred.

The homemade circuit intercepts the data as it is transferred from the data registers to the display and output buffers. The eight digit numbers, background and data, were then sent to the computer.

The signal-to-noise ratio was improved by increasing the number of individual samples and the number of counting cycles. In the threshold region where the percent of electron detachment was low (< 2%), the number of counting cycles effects the signal-to-noise ratio the most. This is due to a decrease in the random noise of the individual samples, which allows for better distinction between two very similar numbers. At large fractional detachment, this was not as important because the signals sufficiently large that the small amount of noise in the background and data counts does not appreciably affect the large difference in the numbers. The signal-to-noise ratio can be increased for large fractional detachment by increasing the number of individual samples. This tends to average the random noise, which improved the signal-to-noise ratio. This technique also raises the signal-to-noise ratio for the small fractional electron detachment, but was not as evident. Obviously, the best situation is to increase the individual samples and the number of counting cycles. This, however, increases the time needed to take each spectral point and, therefore, the entire cross-section spectrum. Other effects, such as ion signal and laser stability, now become important considerations. The problem was solved by taking a large number (20 to 30) of individual samples and modest counting cycles (100 to 200) at electron detachment percentages greater then ca. 5% and taking a lower number of individual samples (10) and

higher counting cycles (500 to 1000) at electron detachment percentages lower than ca. 5%.

The samples at one wavelength made up one spectral point. To determine the EPD spectrum with a specific dye, a number of spectral points (wavelength counts) were taken (usually 150 to 300 points/spectrum). A typical run was 50 to 100 nm in wide.

The wavelength selection was accomplished with the standard Coherent 3-plate birefringent filter that was controlled with a stepper motor (Oriel). After the data at a particular wavelength was obtained, the PC sent a controlled number of pulses to the stepper motor controller which drove the stepper motor and turned the birefringent filter the correct amount to obtain the next wavelength. The number of steps between each desired wavelength was readily controlled.

The laser power was monitored by a power meter (Laser Precision Corp.) which converted the radiant intensity of the photon beam to a voltage. This voltage was sampled by the computer and the wavelength was changed. The intracavity power was measured, after the ion counting had taken place and before the wavelength was changed, using the reflection from the rear FA brewster window.

Because we were concerned with the relative photon in the cavity, and not the absolute power, the amount of reflection from the window need not be known. The percent reflected from the Brewster angle window was constant throughout the wavelength range of a particular dye used. This method of determination was chosen over direct measurement through the high reflective mirror due to difficulties in determining the percent transmission of the mirror at a given wavelength.

The transmission curves of the mirrors were taken on a Cary 14 UV-VIS spectrophotometer. Although the spectrophotometer could determine the transmission to 0.1% accuracy, a determination of 0.01% was needed for accurate EPD cross-section determinations. Most of the transmission curves were estimated accurately enough except for portions in which the transmission changes drastically and in these areas the errors occur. A small error in the transmission of this mirror will result in a large error in the calculated intracavity power.

The percent transmission from the Brewster window was estimated by selecting a wavelength that has a small, but accurately determined transmission, through the high reflective mirror. This determination was made in the middle (flat) wavelength transmission section of the mirrors. The intracavity power was measured through the high reflective mirror using eq. 5. By measuring the intracavity power

$$\text{Intracavity power} = \frac{\text{Cavity output}}{\text{\% reflectance of mirror}} \qquad (5)$$

using the reflectance from the window, the percent reflectance from the window could be back calculated. The reflectance from the mirror was calculated at several wavelengths that the reflectance of the mirror could be determined. The percent reflectance of the window was determined to be approximately 0.1% (0.078 to 0.163%) and was independent of the wavelength. All measurements of laser intensities were made with the same thermopile. Typical powers for the Rhodamine

6G and DCM dyes in the extended cavity range from 10 to 20 watts (590 nm, Rh6G; 640 nm, DCM) with 5 watts pumping from the Ar ion laser. Using higher pumping powers of 10 watts, a intracavity power of 30 to 40 watts was obtained.

The wavelength was monitored by two methods. The first method used of an 1/8-meter monochrometer (Oriel, Model 77250) using the reflection from the birefrigent filter via a small, plastic low grade fiber optic cable (Edmond Scientific) to the front slit of the monochromator. A photodiode detector (Hamamatsu) was mounted in a aluminum housing and placed behind the exit slit of the monochromator. A lens (Oriel, focal length = 15 mm) was also mounted in the aluminum housing and placed at an adjustable distance from the exit slit of the monochromator. The lens was placed at a distance of twice the focal length of the lens from the exit slit so that the image of the slit was reproduced on the small diode detector. The current from the photodiode converted to a voltage using a converter/amplifier (x 10^6 volts per amp) (Analog Modules Inc., model 341-2-d) and monitored with a standard voltmeter (Moconta, model 22-204C). The accuracy of the monochromator was ±0.5 nm, and was found to be extremely reproducible. The accuracy of the monochromator was checked by several sources, e.g. other monochromators and argon pen lamps listed in Table 2.

The second method used to calibrate the EPD spectrum was through the use of an optogalvanic cell. The cell was a hollow cathode

Table 2. Monochromator Wavelength Calibration.

1/8-Meter monochromator(nm)	Ar/Kr Pen Lamp(nm)	3-Meter monochromator(nm)
811.1	811.29	---
759.9	760.10	---
546.4	546.10	---
435.7	435.80	---
404.8	404.66	---
365.1	365.02	---
566.1	---	565.6
566.5	---	566.1
568.0	---	567.5
591.9	---	590.5

discharge tube (Jarrell Ash, tube type 22826; Ne fill gas and a U cathode) obtained from an atomic absorption spectrophotometer. A plasma was developed and maintained inside the cell and the output from the extended cavity was directed into the plasma. This plasma was developed by placing a high voltage (about 400 volts; supplier: Hewlett Packard, model MPB-S/6286A DC) between the anode and cathode, which ionizes the Ne/U mixture. If the wavelength of the laser light corresponds to an absorption or an emission of a species in the plasma the current passing between the plates changes due to changes in the ionization potential of the electronically excited species. The electronic transitions of both Ne and U are known, which gives an

internal wavelength reference from which the monochromator or the EPD cross section spectrum was calibrated. The useful range of the optogalvanic cell was from 550 to 800 nm. The optogalvanic cell spectrum was recorded by taking a scan that was identical to the EPD spectum. This would give an absolute reference for each spectral point. Because the light was chopped, a lock-in amplifier (Princeton Applied Research, model HR-8) was used to monitor the current in the cell. This amplifier monitors the current of the optogavanic cell only while the chopper was open and gives a DC voltage.

I.C.3. Data Acquisition and Cross Section Calculations.

The absorption and ejection of an electron from an anion can be explained from Lambert's law. If we let k_x represent the probability that an ion detaches an electron; $k_x\delta$ is the probability of the detachment in a small amount of time δ. The probability that on ion will not detach an electron is $(1 - k_x\delta)$ and the probability of the ion not detaching over a longer period of time is $(1 - k_x\delta)^n$. If t is the total time, $t = n\delta$, and n is taken to ∞ while holding δ constant the probability that an ion will detach is given in eq. 6. If an ion

$$\lim \left(1 - \frac{k_x t}{n}\right)^n = e^{-k_x t^t} \qquad (6)$$

signal with intensity I_o interacts with a photon beam the probable intensity of the ion signal is given in eq. 7. I/I_o is the fraction of ions that survive the interaction. In the case of EPD k_x is defined in eq. 8. Substitution of eq. 8 into eq. 7 followed by rearrangment an the taking of the logarithm yields eq. 9. Since we can define t as any

$$I = I_o \times e^{-k_x t^{t'}} \tag{7}$$

$$k_x(\lambda) = \xi \times \sigma(\lambda) \times \Phi(\lambda) \tag{8}$$

$$\ln \frac{I}{I_o} = \sigma(\lambda) \times \xi \times \Phi(\lambda) / t^{t'} \tag{9}$$

length, t′ is then 1. Rearranging eq. 9 to obtain $\sigma(\lambda)$, which represents the loss of an ion due to EPD as a function of wavelength (energy), eq. 10 is obtained;[35, 33a] I and I_o are the intensity, or

$$\sigma(\lambda) = \frac{\ln(I_o/I)}{\Phi(\lambda)} \times \frac{\xi}{t} \tag{10}$$

the ion counts measured with the laser-on and the laser-off, respectively, ξ was the geometric constant describing the overlap between the photon beam and the ion swarm that was monitored by the mass spectrometer, t was the mean time the ion spends in the photon beam, and $\Phi(\lambda)$ was the photon flux. Because both t and ξ are difficult to determine and are constant during the determination of one dye's spectrum, as was their ratio, they can be ignored to determine $\sigma_{rel}(\lambda)$. Therefore, eq. 6 is transformed into eq. 7. The ion counts measured with the laser-on, laser-off, and the power

$$\sigma_{rel}(\lambda) = \frac{\ln(I_o/I)}{\Phi(\lambda)} \tag{11}$$

of the beam combined with the beam diameter (the photon flux) are required to calculate a relative cross section. To calculated the photon flux, the photon beam intensity was measured as previously described. Equation 8 was used to calculate $\Phi(\lambda)$ (unit = photons/sec

per unit area(mm)). The last two terms term converts the intensity from J sec^{-1} to eVs.

$$\Phi(\lambda) = \frac{\text{Photon beam intensity(J sec}^{-1})}{1\ \text{mm}^2} \times \frac{1\ \text{eV}}{1.6 \times 10^{-19}\text{J}} \times \frac{1\ \text{photon} \times \lambda}{1239.9\ \text{eV}} \qquad (12)$$

The photon beam cross sectional area was assumed to be 1 mm^2. This assumption need not be held strictly due to the determination of relative cross section. In fact, the photon flux or the photon beam intensities need not be calculated since the voltage from the thermopile was sufficient to calculate the relative cross section. If the absolute cross section was to be calculated, the absolute photon flux would need to be determined by accurate measurements of the beams cross sectional area and intensity. A second assumption made was that the beams cross sectional area remains constant during a spectral run. The calculated relative cross section was related to all other relative cross sections within one spectral run and if the photon beam diameter was to change than this relationship, or relativeness, to the other spectral points would also change.

To verify the EPD was a single photon process, the cross section at a single wavelength was determined as a function of the intensity (Figure 5). The data showed a linear relationship. If the EPD process was a higher order photon process a linear relationship would not be observed.

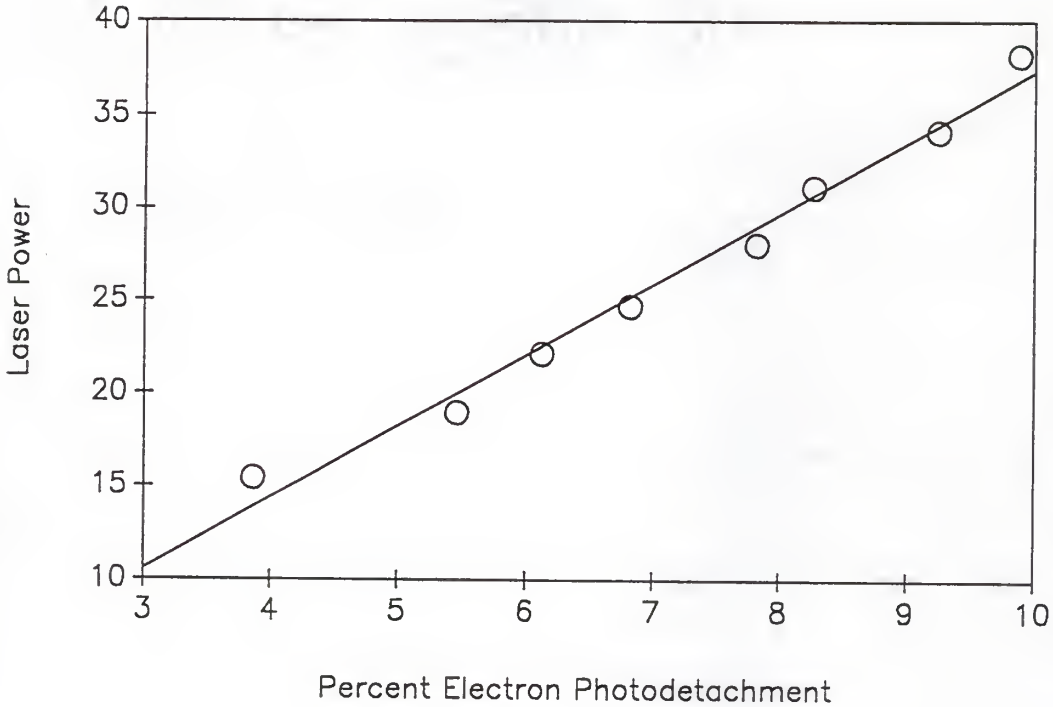

Figure 5. Plot of laser power vs. percent EPD. A linear relationship shows a one photon process.

Data were stored by a Zenith Z-158 PC/XT computer. The acquisition routines were written in Quick Basic 4.0 and were run in the compiled form. The digital data from the photon counter was taken with digital interface card (Metrabyte, model PIO-12) while the analog data (power meter, stepper motor control, and the optogalvanic cell) were taken via a analog input/output interface card (Metrabyte, model DASH-8).

The program that acquired the data served several functions. These are presented in a sequential order. The program first inquires for the specifics of the spectral run, i.e. output file name, location of output file (either the hard disk drive with the correct path or a

floppy disk drive), the number of spectral points to be taken, and the starting number of the spectral run. This allows for the customizing, systematizing, and cataloging of the data. The program would send a command to the home-made photon counter circuit to clear its memory and start acquiring data, and waits for laser-on and laser-off data pair to be exported from the PIO-12 digital interface card. These numbers, once acquired, would be placed into the file (preceded by the spectral point number) named at the beginning of the spectral run along with the calculated percent difference between the background and data. The voltage was then acquired from the laser power meter and exported to the named file. The program then sends a predetermined number of pulses to the stepper motor controller. These pulses were determined before the run by trial and error so that the spectral points would be of the desired spacing. This was done for each dye.

The trial and error determination for pulse calibration consisted of sending a number of pulses to the stepper motor controller after having noted the starting wavelength. When the stepper motor had completed the number of steps the final wavelength was determined. The number of pulses per nanometer (nm) was calculated by dividing the number of pulses sent to the stepper motor controller by the the change in wavelength as a result of those pulses to give the pulses/nm. Multiplying the pulses/nm by the nm/spectral point desired, the pulses sent to the stepper motor controller/spectral point were calculated. Typically the number of pulses to the stepper motor was 25 to 40 and was constant within a particular dye. However, if the dye was changed, then the pulse calibration must be determined for the new dye.

Finally the program returns to the start of the acquisition routine and clears the memory and acquires the data once again. The acquisition routine was repeated the number of times specified by the initial "number of spectral points to be taken" value.

The EPD data files were saved in ASCII files, which, were imported into a Lotus 2.0 spreadsheet for calculation and analysis. The data files contained five columns of information. The first was simply the spectral point number. The second column contained the averaged background (laser-off) counts while the third was the averaged data (laser-on) counts for each spectral point. The fourth column was the percent difference between the laser-off and laser-on counts, while the fifth column was the voltage from the laser power meter, which ranged from 0 to 1 volt. By knowing to which scale the laser power meter was set, the absolute laser power inside the cavity was calculated. As mentioned previously, the absolute laser power inside the cavity was not necessary and the voltage could be used directly; the absolute laser power was calculated and used. For analysis purposes, the laser power meter scaling factor from the power meter was always recorded and used. The spreadsheet first calculated the intracavity power assuming that the reflectivity of the window was 0.1%. This was done by multiplying the voltage reading by the scaling factor, which gives the intensity measured by the laser power meter, and then dividing by 0.1%. This power was used to calculate the photon flux, $\Phi(\lambda)$, and the cross section, $\sigma(\lambda)$.

A previous group[33a] used a functional form (eq 9) to calculate the circulating intracavity power, $P_c(\lambda)$, that differs from the calculation

used in this experiment. In eq. 9, $P_0(\lambda)$ is the laser output power,

$$P_c(\lambda) = \frac{P_0(\lambda)\ [2 - T(\lambda)]}{T(\lambda)} \tag{9}$$

$$P_c(\lambda) = \frac{2 \times P_0(\lambda)}{T(\lambda)} \tag{10}$$

and $T(\lambda)$ was the transmission of the high reflective mirror. Since $T(\lambda)$ was small, 0.01, $2 - T(\lambda)$ reduces to two. This was shown in eq. 10, which was the same form used in this experiment multiplied by two. The factor of two arises from the definition of the intracavity power. Equation 9 treats the photon beam as a particle that travels from a starting point down the length of the cavity through the interaction region, was reflected from the high reflective mirror, passes again through the interaction region, and back down the length of the cavity back to the starting point. This completes one round trip. The $2 - T(\lambda)$ arises from the two possible chances for ion interaction for each photon that travels the round trip minus the small amount of photons that make only one half of the round trip due to their passing through the high reflective mirror. Since $T(\lambda)$ was small, eq. 9 was reduced to eq. 6. The present experiment treats the laser cavity as a standing wave and treats the intensity as a electromagnetic wave. Thus, the "photons" interact with the ions once. Both forms yield identical EPD spectrum.

A scaling of the EPD spectra to values between zero and one was done. This was accomplished by setting the largest number for the calculated $\sigma_{rel}(\lambda)$ equal to one and then multiplying the other numbers

in the EPD spectrum by the same factor. This does not change the relative cross section vs. λ spectrum, but allows for numbers that are in accord with other dyes EPD spectra.

To determine the λ at which the experimental EPD cross sections go to zero, each curve was fit to the threshold law (eq. 11) developed by

$$\sigma(E) = E(E-E_0)^{3/2}[A_0+A_1(E-E_0)+A_2(E-E_0)^2+.....] \qquad (11)$$

Geltman[36,37] for an ion having "symmetric σ, π, or δ orbitals". In this polynomial expansion, E is the photon energy, E_0 is the energy at the threshold, and A_n are constants. This expression with six A_n terms was used to calculate the EPD onset. The data analysis was very sensitive to the number of points used. For $\underline{c}$-$C_5H_5^-$ and $\underline{c}$-$C_5H_4^{\bullet -}$, only the first 30 to 40 nm above threshold were used to fit the data. The 40 nm value was determined by starting with small data sets and fitting the data with the expression. As the number of points was increased, the correlation (in this type of analysis the Sum of the Root Squares; SRS will decrease) between known points of the onset and the values calculated by the threshold law became low. If too many points were used, the calculated threshold would be at a wavelength at which the EPD spectrum was obviously not zero. If to few points were used, the calculated onset wavelength would be too low in energy. For this reason all threshold law fits to the data must be treated with caution.

To identify additional transitions involving electronic or vibrational states in the slowly rising EPD cross section vs. λ spectra, the derivative of the spectra were taken. This was

accomplished using a program written by P. M. A. Sherwood.[38,39] In this method, the data points are first fit to the general formula given in eq. 12. In this formula, y(0) was the point to be fit (or smoothed) which corresponds to the center of an odd number points, f(t)

$$y(0) = \sum_{-m}^{m} \frac{C \cdot f(t)}{NORM} \qquad (12)$$

are experimental data points in the given interval, C is a convoluting integer, and NORM was a normilization factor. Both C and NORM are calculated by the program. The function was derivitized and the data points calculated. If structure was indicated, the data points for each individual dye, if several dyes were used to determine the range of the spectrum, was differentiated separately. This was done to be certain that the structure was genuine and not an artifact of the splicing together of the separate dye runs. A sample of both type of derivative analysis was presented (see figures 13, 14, and 15), were applicable, with the results.

I.C.7. Artifacts

Several problems were identified in the development of this experimental method. The first had to do with the presence of free electrons in the downstream flow resulting in a vertical offset of the EPD spectrum. This was discovered by finding no EPD at a wavelength where EPD was known to occur. Specifically, when acetophenone enolate anion was formed in the presence of excess free electrons in the flow, a EPD spectrum passed though the zero at 614 nm and continued to fall

below zero at longer wavelengths. Several experiments were carried out to determine what the effect of the electron guns emission current was on this offset. These studies involved varying the electron guns emission current, adding SF_6 at the neutral inlet to detect free electrons ($SF_6 + e^- \rightarrow SF_6^-$), and then determining the EPD spectrum of acetophenone enolate anion. It was found that the offset was not directly dependent on the electron guns emission current, but was caused by free electrons in the helium/acetophenone enolate anion flow when the interaction with the photon beam occurred. The free electrons downstream had no effect on the relative cross sections except they were shifted vertically, either positively or negatively. An example of a positive offset is shown in Figure 6. As a result of this discovery, all spectra were aquired after the free electrons had been removed from the flow in the upstream end of the flow tube.

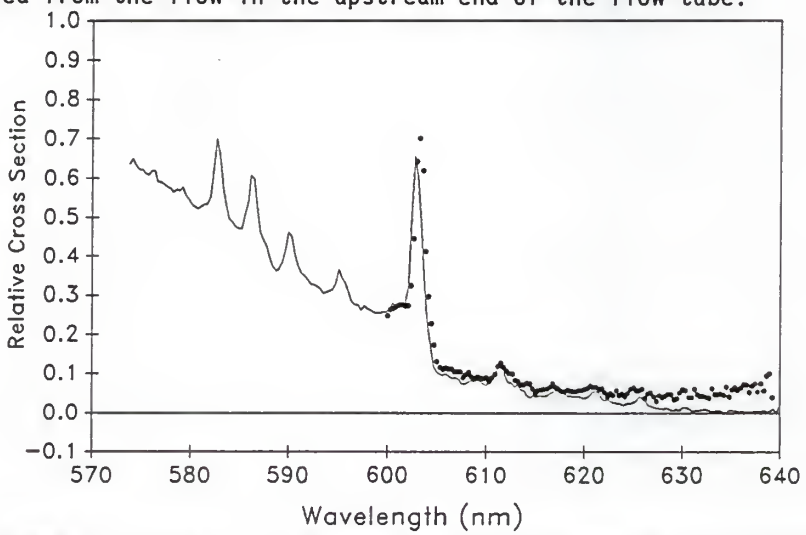

Figure 6. Offset of EPD spectrum of acetophenone enolate anion. The solid line(-) represents the known EPD spectrum. The dots (•) are the EPD spectrum when free electrons were present downstream.

Another associated problem was the control of the amount of ion neutral precursor added to the flow. If two much of the precursor was added, the EPD spectrum could be offset in either a positive and negative direction. In the case of the EPD spectrum of $\underline{c}$-$C_5H_5^-$, this was not a problem. However, this problem was observed in the determination of the EPD spectrum of acetophenone enolate anion. This anion was formed by proton abstraction from acetophenone by preformed F^-. If too much acetophenone was added to the flow, the spectrum would be offset. To eliminate this problem, the amount of acetophenone was carefully controlled so that only enough was added to fully remove the F^- ion signal. Neither situation effected the relative cross section vs. λ spectrum except it was offset. No offset was observable if a small amount of the F^- remained in the flow.

In the determination of the EPD spectrum of $\underline{c}$-$C_5H_4^{\bullet -}$, a precursor concentration complication was due to the reaction of the anion radical with additional diazocyclopentadiene precursor yielding the azine anion radical $(\underline{c}\text{-}C_5H_4\text{=N-N=}\underline{c}\text{-}C_5H_4)^{\bullet -}$ at m/z 156. The azine anion radical apparently photodissociated to give the $\underline{c}$-$C_5H_4^{\bullet -}$ and $\underline{c}$-$C_5H_4N_2$. Thus, the resulting cross section was a combination of the EPD of $\underline{c}$-$C_5H_4^{\bullet -}$ and photodissociation of the azine anion radical. This problem was eliminated by adding only small amounts of the diazo compound via inlet 1, which was accomplished by loading a portable 5-L gas bulb with 1-2% $C_5H_4N_2$/He and controlling the amount added at inlet 1 with a small stainless steel needle valve.

Another observed anomaly was that the amount of EPD for all of the negative ions investigated at a given wavelength was a function of the

nose cone potentials. While the exact nature of this anomaly remains unknown, it can be controlled and used to increase the signal to noise ratio. The effect was such that as the potentials that are placed on the first nose cone and its aluminum holder are varied, the percent EPD also varies. If the first nose cone potential was raised from -(1 to 2) to -(5 to 7) volts and the nose cone holder potential was dropped from -24 to -(12 to 15) volts, the ion signal will decrease by 25%, but the percent EPD will increase from 1 to 15% to as much as 40 to 50% at the same wavelength. The relative EPD spectrum was unchanged but the signal-to-noise ratio was greatly improved. The exact values of these potentials vary from spectral run to spectral run and no apparent trend in terms of signal to potential was obvious.

It was suggested[40] that this nose cone potential anomaly may due to a change in the velocity of the ions to be sampled through the nose cone orifice. As the ion plasma exits the flow tube (see Figure 3), the plasma changes direction being drawn upward as the flow leaves the first compartment toward the large, fast pumping system. The ions to sampled are derived from the sheath of the plasma. As the potential on the aluminum nose cone holder is made more positive (less negative), the negative ions velocity increasw which reduces the cone angle for the sampled ions through the extended cavity laser beam even though the total sampled ion signal decreases. This corroborates the ideas advanced in this laboratory.

As a result of these artifacts, each spectral run must be checked for (a) no free electrons downstream, (b) large excesses of neutral

precursors are not present in the flow, and (c) the percent EPD was as high as possible without large losses of ion signals.

I.D. Materials

I.D.1. Generation of Acetophenone Enolate Anion in a FA.

Acetophenone (supplier: Aldrich) was distilled (b.p. 200.5 to 204°C, 760 torr) and a constant boiling fraction was placed in a finger for inletting into the flow tube via inlet 2. Flouride ion was generated in the Pyrex glass side-arm by DEA with NF_3 (Ozark Mahoney) added via inlet 1. The electron guns emission current was kept low, typically 50 to 200 μA, to ensure that no free electrons were downstream. The absence of electrons after inlet 4 was verified by adding SF_6, which has a high electron attachment cross section; no signal for SF_6^- was observed. The F^- reacted with acetophenone to produce the acetophenone enolate anion and HF. Only enough acetophenone was added to remove the F^- signal. No other anions were observed in the flow. The EPD experiments were then carried out on the ion.

I.D.2. Generation of Cyclopentadienyl Anion.

Cyclopentadiene was obtained by thermally cracking the liquid dimer (supplier: Aldrich) and collecting the middle fraction. Two gas-phase methods were used to generate the cyclopentadienyl anion, $\underline{c}$-$C_5H_5^-$. The first was proton abstraction from the neutral precursor by CH_3O^-.[41,42] The precursor of the base, CH_3ONO, was synthesized by Cheng Tung.[43] In a flask is placed 72.5 g (1 mole) of NaNO, 45 mL (1.125 mole) of CH_3OH, and 42.5 mL of H_2O. The flask was fitted with a dropping funnel containing 113.75 mL of cold dilute H_2SO_4 (1:2 ratio mixed with water). The acid is added dropwise to the stirred solution and the gaseous CH_3ONO was passed through Na_2SO_4 to remove water. The clean, dry CH_3ONO was then condensed into a finger cooled by liquid

nitrogen. CH_3ONO was inletted into the flow tube via inlet 1 and underwent DEA to produce CH_3O^- and NO. $\underline{c}$-C_5H_6 was added via inlet 2 and proton transfer occurred with the CH_3O^- to produce $\underline{c}$-$C_5H_5^-$ and CH_3OH. Just enough C_5H_6 was added to remove the CH_3O^- ion.

The other method used was direct DEA of $\underline{c}$-C_5H_6 to produce $\underline{c}$-$C_5H_5^-$ and H-atoms. No other ions were present and no electrons were detected downstream with added SF_6. Both methods gave identical EPD spectra.

I.D.3. Preparation of diazocyclopentadiene.

The diazo compound was prepared from the procedure described by Doering and DePuy.[44,45] Phenyllithium (supplier: Aldrich) (500 ml of 2M, 0.5 moles) was placed in a three neck flask. To this, 33 mL (0.62 moles) of freshly distilled cyclopentadiene was added dropwise over a period of 30 min. The resulting solution was magnetically stirred for another hour. The solution of $\underline{c}$-$C_5H_5^-$ was then forced under N_2 pressure (850 torr) though a tube into a flask containing a cooled solution of 100 g (0.55 moles) $\underline{p}$-toluenesulfonyl azide in 300 mL of dry ethyl ether with magnetic stirring. The base was added in a slow and continuous manner over one hour to maintain a gentle reflux of the ether solution. The solid that is formed during the addition was filtered from the solution containing the diazo compound. The filtrate was then washed three-times with 10 mL portions of water and dried over sodium sulfate. The diluted diazo was be purified by either of two methods.

The first method was that which is described by DePuy.[48] The diazo solution was distilled at a pressure of 50 mtorr and the fraction that

boiled from 45 - 55 °C was collected. This procedure produced several small explosions and one rather large one.[46] It was deemed that an alternative method for the purification was necessary.

The second method for the purification of the diazo was to forgo the initial distillation and proceed directly to a low temperature crystallization.[48] Small portions of the diazo solution was added to hexane which was cooled in an acetone/Dry Ice bath to allow for the solid diazo to form. The hexane was removed by pipette and the diazo compound was vacuum dried at 50 mtorr. The ^{1}H NMR showed only benzene as an impurity. This was removed by placing the cold solid diazo in a vacuum (50 mtorr) for about 5 min. The ^{1}H NMR (δ 6.0 (2 H), 6.85 (2 H) and the IR (2250 cm^{-1}) spectra were consistent with diazocyclopentadiene.

I.D.4. Generation of Cyclopentadieneylidene Anion Radical.

The generation of c- $C_5H_4^{\bullet -}$ was accomplished by DEA with diazocyclopentadiene.[12] c-$C_5H_4N_2$ was added via inlet 1. The electron gun current was kept as low as possible (50 to 300 μA) to minimize the number of electrons downstream. Several problems arise from the generation of this species. If too much of the diazo compound was added, several ions were produced. The primary ion was $C_5H_4^{\bullet -}$ (m/z 64), while the secondary ion products were cyclopentadienone azine anion radical (m/z 156) (eq. 13a), the pentafulvalene anion radical (m/z 128) (eq. 13b), and cyclopentadienyl anion (m/z 65) (eq. 13c). The fast rate of these secondary reactions (k_{total} = 4.4 x 10^{-10} cm^3

molecule^{-1} sec^{-1})[12] caused the rapid loss of the signal for the primary ion $\underline{c}$-$C_5H_4^{\bullet -}$.

$$\underline{c}\text{-}C_5H_4^{\bullet -} + C_5H_4N_2 \xrightarrow{0.62} (\underline{c}\text{-}C_5H_4)N_2(\underline{c}\text{-}C_5H_4)^{\bullet -} \quad (m/z = 156) \quad (13a)$$

$$\underline{c}\text{-}C_5H_4^{\bullet -} + C_5H_4N_2 \xrightarrow{0.29} (\underline{c}\text{-}C_5H_4)=(\underline{c}\text{-}C_5H_4)^{\bullet -} \quad (m/z = 128) \quad (13b)$$

$$\underline{c}\text{-}C_5H_4^{\bullet -} + C_5H_4N_2 \xrightarrow{0.09} \underline{c}\text{-}C_5H_4^{-} \quad (m/z = 65) \quad (13c)$$

Another problem is that the azine anion radical (m/z 156) underwent photodissociation at wavelengths employed (550 to 720 nm) to generate c-$C_5H_4^{\bullet -}$. This is represented in eq 14a. This was

$$(\underline{c}\text{-}C_5H_4)N_2(\underline{c}\text{-}C_5H_4)^{\bullet -} + h\nu \longrightarrow \underline{c}\text{-}C_5H_4^{\bullet -} + C_5H_4N_2 \quad (14a)$$

$$\underline{c}\text{-}C_5H_4^{\bullet -} + h\nu \longrightarrow \underline{c}\text{-}C_5H_4^{\bullet -} + e^{-} \quad (14b)$$

determined by forming a large signal for the ion at m/z 156 and allowing the ion to interact with the photon beam (eq. 14b). The large loss of ion intensity and the increase of the signal intensity for $\underline{c}$-$C_5H_4^{\bullet -}$ suggested that eq. 14a was true. The photon beam had no effect on the ion at m/z 128. The carbene anion radical formed by the photodissociation of m/z 156 will then undergo EPD. The cross section for the photodissociation of the azine appears to be large due to the loss of >50% of its signal at 600 nm. The condition of primary importance is the inlet of very small amounts of a 1-2% $\underline{c}$-$C_5H_4N_2$/helium mixture via inlet 1. The mixture of diazo/helium was accomplished by loading a 5-L bulb with 30 mtorr of the diazo compound and dilution with helium. This bulb was used as the diazo source and allowed fine control of the amount of diazo compound added into the flow, which

allowed for the generation of the c-$C_5H_4^{\bullet -}$ (m/z 64) in the absence of the secondary ions at m/z 156 and 128.

It was previously determined from ion/molecule chemistry that the skeletal structure of m/z 64 was the cyclic five-membered ring and not an isomeric species.[12] The ion at m/z 64 was generated and allowed to undergo H-atom with CH_3OH to yield the ion at m/z 65. The reactions of $\underline{c}$-$C_5H_5^-$ (formed by $\underline{c}$-C_5H_6 + CH_3O^-) have previously been characterized.[47] The product of $\underline{c}$-$C_5H_4^{\bullet -}$ reacting with CH_3OH was then subjected to these same reactions.[48] In all cases, the rate constants and products were identical.

I.D.4 Preparation of Dye Solutions.

The three dye solutions used in this study were prepared by dissolving the appropriate solid dyes (Exiton) in the corresponding primary solvent then diluting the concentrated solution of the dye with ethylene glycol. Both Rhodamine 6G or Rhodamine 110 (approximatly 0.65 g) were dissolved in 300 mL of spectroscopic grade methanol and magnetically stirred for 20 min. To this solution was added 700 ml of ethylene glycol slowly. Constant stirring assured adequate mixing. The solution of the dye was then transferred to the dye laser pump module. To obtain the highest power from the dye laser, the concentration of the solution was adjusted by adding additional dye (a small portion of the dye dissolved in a minimum amount of methanol), a procedure called "spiking", or pure ethylene glycol to the pump reservoir. This optimized the concentration of dye. Small portions (1 - 2 mL) of the concentrated dye were added; if the output of the dye laser decreased, small portions of ethylene glycol were added until the

power was maximized. If the concentrated dye solution was added the power increased, additional dye solution was added to maximize the dye laser power.

The solutions of DCM were more difficult to make. Approximately 0.6 g of this dye and 300 mL of benzyl alcohol were placed in a 500 mL Erlenmeyer flask and placed in an ultrasonic bath. About 45 min in the bath was sufficient to effect solution. To this solution 700 mL of ethylene glycol was added slowly (45 min) due to problems of the dye crystallizing in the dye storage container. The dye concentration was optimized as above.

I.E. Results and Discussion.

Because electron photodetachment (EPD) cross sections had not been previously determined using a flowing afterglow (FA) apparatus, several control studies were done to characterize the reproduciblity of spectral features and the accuracy of the electron affinities (EA) determined. The two organic negative ions selected for this purpose were actophenone enolate anion ($C_6H_5C(O^-)=CH_2$) and cyclopentadienyl anion ($\underline{c}$-$C_5H_5^-$). The EPD spectrum of $C_6H_5C(O^-)=CH_2$ had been determined in an ion cyclotron resonance spectrometer using a laser system by Brauman's group at Stanford.[49,50] To reproduce the various resonances reported for this negative ion at and near the $0 \leftarrow 0$ EPD transition was considered to be a model test for our FA/laser system.

To further determine the accuracy of the EAs of the neutral molecules determined by the threshold of EPD of the corresponding negative ions $\underline{c}$-$C_5H_5^-$ was the second anion investigated. Lineberger, et. al.,[51] had reported the EA($\underline{c}$-C_5H_5) determined by photoelectron spectroscopy (PES). PES is considered by most scientists to be the most accurate method to determine such data. The $\underline{c}$-$C_5H_5^-$ is also related structurally to the target negative ion of these studies, cyclopentadienylidene anion radical ($\underline{c}$-$C_5H_4^{\bullet -}$).

I.E.1. Determination and Interpretation of the Electron Photodetachment Spectrum of Acetophenone Enolate Anion.

Brauman, et al.[49,50] first determined the EPD cross section vs. λ spectrum of $C_6H_5C(O^-)=CH_2$ in 1977 using an ion cyclotron spectrometer (ICR) employing both low resolution (23 nm fwhm) (FIgure 7) and high resolution (0.25 nm fwhm) (fig. 8) light sources. The low resolution

spectrum exhibits a broad maximum at $\lambda_{max} \approx 450$ nm. To determine if this maximum was due to a electronic transition, Brauman[50] studied the effect of several π-donating and π-accepting p-substituents on the spectrum. For the π-donating groups, F, CH_3, and tert-butyl, position

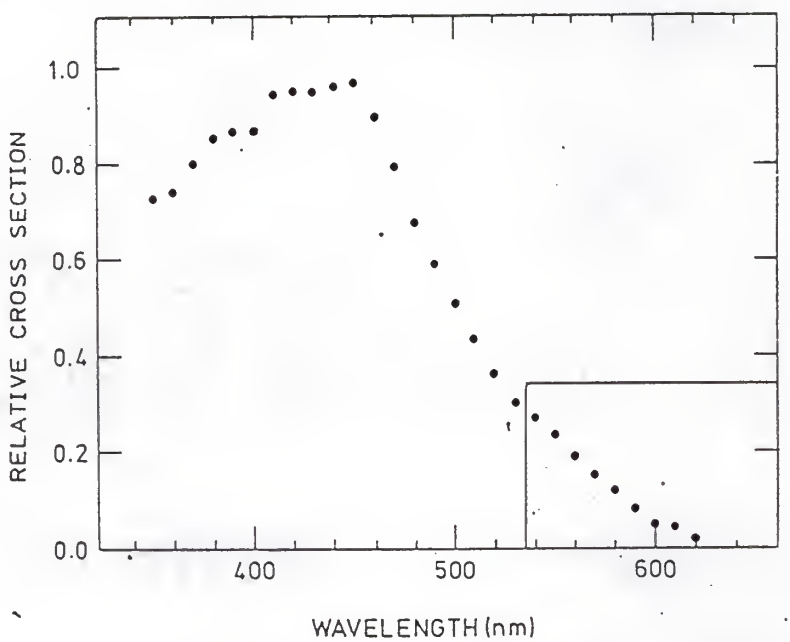

Figure 7. Relative EPD for acetophenone enolate anion determined by ICR (resolution: 23 nm fwhm).[49,50]

the effect was a blue shift (a shift to lower wavelengths) in the low resolution EPD λ_{max} with F > CH_3 > t-butyl. Such shifts were expected from CNDO/2 calculations on the anions where the π^*-MO shifts to higher energy and the energy required for the electronic transition increased. A π-accepting p-cyano group caused a red shift because the energy of the π^*-MO was lowered.

To resolve the question as to the nature of the transition ($n \rightarrow \pi^*$ or $\pi \rightarrow \pi^*$) the molecule was considered to be one of the general class $C_6H_5C(=O)X$, where X is NH_2, CH_3, and Cl. Calculations show that as the π-donating ability of X increased, the transition would favor the $\pi \rightarrow \pi^*$.[52] For example, with X = CH_3, the weakest π-donor, the transition is $\pi \rightarrow \pi^*$. With X = NH_2, the $n \rightarrow \pi^*$ transition is favored for this strong π-donator. For the anion X = CH_2^-, the expected transition should be the $\pi \rightarrow \pi^*$ due to the strong π-donation by CH_2.

The EPD spectrum was determined at high resolution in the ICR (Figure 8) by employing a laser beam near the wavelength of the EPD threshold. The high resolution EPD spectrum was also determined in the present FA/laser system (Figure 9). The two determinations show excellent agreement and several sharp resonances are seen in both EPD spectra. The assignment of these resonances and the origin of the red tail must be determined to correctly identify the EPD threshold. The CNDO/2 calculations show that electronic states at lower energy than the transition at $\lambda_{max} \approx 450$ nm. This conclusion was verified by the absence of substituent effects in the ring on the energy spacings, $\delta\lambda$, on these transitions even though the overall spectum did exhibit substitution effects. That these transitions imposed on the rising continuum of the EPD cross section vs. λ spectrum were not rotational in character was concluded from the widths of the observed resonances; rotational transitions would have widths much less than those observed.

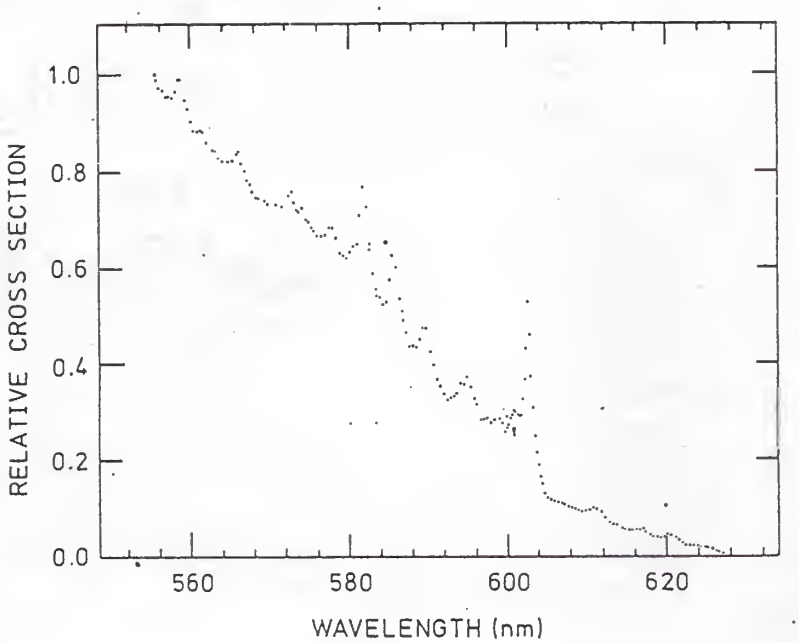

Figure 8. Relative EPD for acetophenone enolate anion determined by ICR. (resolution: 0.25 nm fwhm).[49,50]

The lifetimes of the resonant states can provide insight into the coupling of the resonant state to the continum and, therefore, possible vibrational state assignments of these resonances. The resonant state lifetime was estimated from Fano line shape analysis to be 10^{-12} to 10^{-13} sec which corresponds to several vibrational periods. If the excited state of the radical plus the electron lies lower in energy then the threshold, poor coupling would result since a vibrational to electronic energy transfer would be necessary for autodetachment.[49,50] The energy could come from two sources. The first is off diagonal

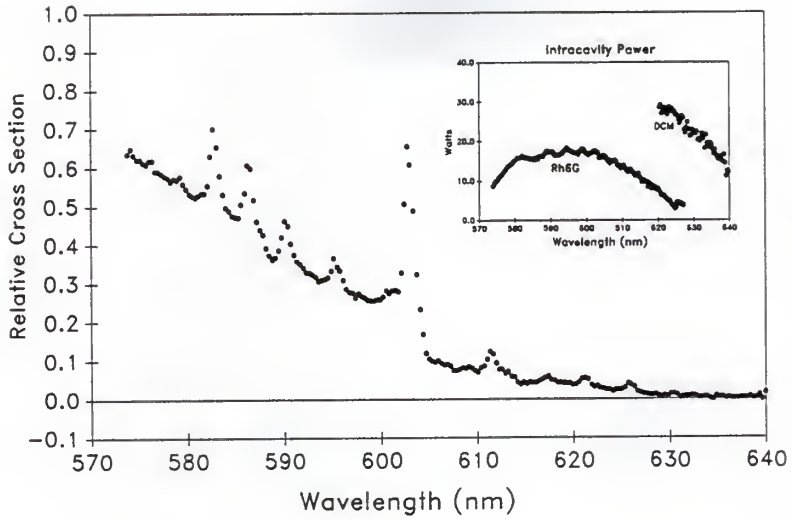

Figure 9. Relative EPD spectrum for acetophenone enolate anion determined in the FA (resolution 0.25 nm fwhm).

transitions to the resonant states vibrational manifold. The second is a transition from vibrationally excited ions. In the latter case, the widths of the peaks should vary by no more then an order of magnitude with the degree of vibrational population which is the case. If the resonant state lies just below the threshold, it would take only a few vibrational periods for energy transfer from vibrational levels of the resonant state for autodetachment to occur. This point indicated that the resonant state was, in fact, a bound state of the ion since an unbound state would have a shorter lifetime.

One possibility[53,54] for the nature of this bound state was the dipole supported state advanced by several scientists.[55,56] These

studies show that an electron in a fixed field has an exact quantum mechanical solution and a neutral molecule with a substantial dipole moment could be the fixed field. It was shown that the critical value of the dipole was 1.625 D. Above this value, an infinite number of states exist and converge to the continuum. These dipole supported states would dominate at low electron energies, since the interaction would be large enough to neglect electron correlation. This neglect may not be possible since the lowest energy electron/dipole state is largest at the center of the dipole[57] which is where electron correlation cannot be neglected.

In fact, this simple model describes highly polar molecules rather poorly. Jordan and Wendolski[58] performed ab initio calculations on organic molecular negative ions whose dipole moments ranged from 2 to 5 D. The calculations indicated that the ions had slightly bound excited states whose wave functions were similar to those for the dipole model. However, the calculations gives poor EAs.

Rohr and Linder studied the low energy electron scattering cross sections for HCl and HF,[59] which show resonances for vibrational excitation that do not correlate to any know states of HCl^- or HF^-. These resonances were attributed to a dipole supported states which suggest that while the simple electron/dipole model is important, the critical value of 1.625 D cannot be accurately determined. This arises from the fact that $\mu_{HCl} < \mu_{critical}$ while $\mu_{HF} > \mu_{critical}$.

Wong and Schultz investigated the scattering cross section of CO^{-}[60] and found a resonant peak a $\approx$ 6 eV. At the time the peak was attributed to a state the is coincident with the $a^3\pi$ state of CO.

However, when N_2, an isoelectronic model with no dipole moment, was investigated no peaks were observed. The peak found in the CO^- spectrum is now assumed to be a dipole supported state.

Dude and Herzenberg modified the calculation which discribed the interaction near the center of the dipole.[61] The method was used to calculate the cross sections vs. λ spectra which strongly resembled the experimental results and provides convincing quantitative evidence for electron/dipole supported states.

The conclusion was drawn that the resonant peaks in the acetophenone enolate anion result from a dipole supported state.[53,54] While the dipole moment for the radicals is unknown, a reasonable assumption is that the dipole will not differ significantly from that of the parent carbonyl compound of 3.02 D.[62] Which is reasonable for a dipole supported state.

The above discussion led to Brauman, et al. to assign the sharp peak centered at 602.6 nm to the 0 ← 0 vibrational transition that corresponds to the adiabatic electron affinity of the radical, $C_6H_5C(O)CH_2\bullet$. Because the 0 ← 0 transition is has a strong Frank-Condon factor, it is much larger than all other resonant peaks and was assigned to this transition.[49] If the 0 ← 0 transition had been obscured by rotational bands, the EA would be difficult to determine. An EPD study of acetaldehyde enolate anion suggested that the EA of the radical occurred at this resonant peak.[63]

The smaller resonant peaks at high energy than the 0 ← 0 transition were assigned to the vibrational progression of the dipole

supported state. The assignment of individual energy levels was not possible due to the size of the molecule.

The foot transitions observed at lower energy than the 0 ← 0 transition were attributed to vibrationally excited anions of acetophenone enolate anion. If these levels could be further populated, a increase in their relative intensities should be observed. This was attempted by generating F^- and allowing it to be carried down the flow tube and adding acetophenone at the last accessible inlet. The flow velocity was also increased to improve the possibility of observation of vibrationally excited acetophenone enolate anions before entering the photon beam interaction region. Under these conditions, $\underline{v}$ > 80 m/s, P_{He} = 0.5 torr, and 298 K, the number of stabilizing collisions with the helium buffer gas would be minimized due to a large number of stabilizing collisions even under these conditions. All attempts to significantly populate the vibrationally excited levels of the anion apparently failed since no change in the relative intensities of the lower energy transition was observed.

I.E.2. Determination and Interpretation of Electron Photodetachment Spectrum of Cyclopentadienyl Anion.

The ability of the FA/laser system to resolve vibrational structure was established with the EPD spectrum of acetophenone enolate anion. The next question to address was the accuracy of the EPD threshold measurements for cases without structure. To answer this question. It was decided to determine the EPD spectrum of $\underline{c}$-$C_5H_5^-$. The EA($\underline{c}$-$C_5H_5^-$) had been reported using photoelectron spectroscopy (PES).[64] The symmetry of the radical $\underline{c}$-$C_5H_5\bullet$ precluded the presence

of a dipole supported state. Thus, the EPD threshold should be clearly observed. Photodetachment of a π-electron from $\underline{c}$-$C_5H_5^-$ yielding $\underline{c}$-$C_5H_5\bullet$ was considered to be similar to that expected for EPD of $\underline{c}$-$C_5H_4^{\bullet -}$ producing ground state triplet carbene $\underline{c}$-C_5H_4, the target for this study. Therefore, similarities in the EPD spectrum for $\underline{c}$-$C_5H_5^-$ and $\underline{c}$-$C_5H_4^{\bullet -}$ were expected.

The π-molecular orbitals of $\underline{c}$-$C_5H_5^-$ and $\underline{c}$-$C_5H_5\bullet$ are shown in Figure 10. The degeneracy of ψ_2 and ψ_3 in the anion is allowed because of the planar configuration. Ejection of an electron from either ψ_2 or ψ_3 of the anion removes this degeneracy because Jahn-Teller distortion of and the corresponding orbitals in the radical are of different energies. This geometry change in $\underline{c}$-$C_5H_5\bullet$ is called a Jahn-Teller

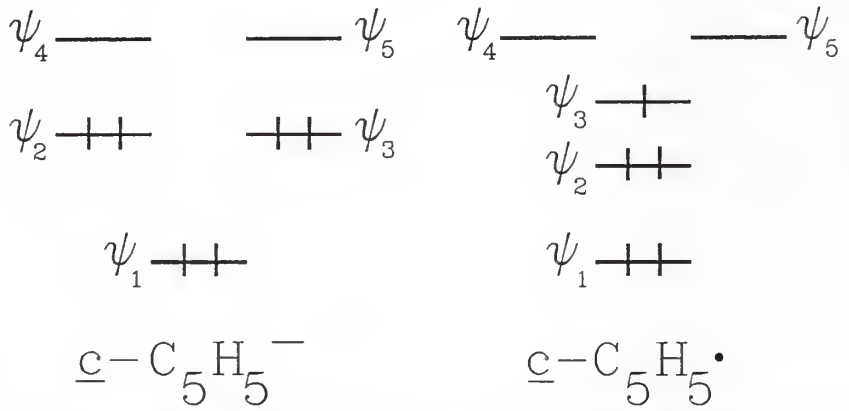

Figure 10. π-Molecular orbital and relative orbital energy diagrams of $\underline{c}$-$C_5H_5^-$ and $\underline{c}$-$C_5H_5\bullet$.

distortion. To determine the adiabatic EA of the neutral, the transition from the ground state of the anion must go to the ground state of the neutral. The question is then to determine if the

geometry change are large enough to preclude observing the 0 ← 0 transition.

As mentioned previously, Linberger, et al., determined the photoelectron spectrum of $\underline{c}$-$C_5H_5^-$ (Figure 11).[68] The electron energy

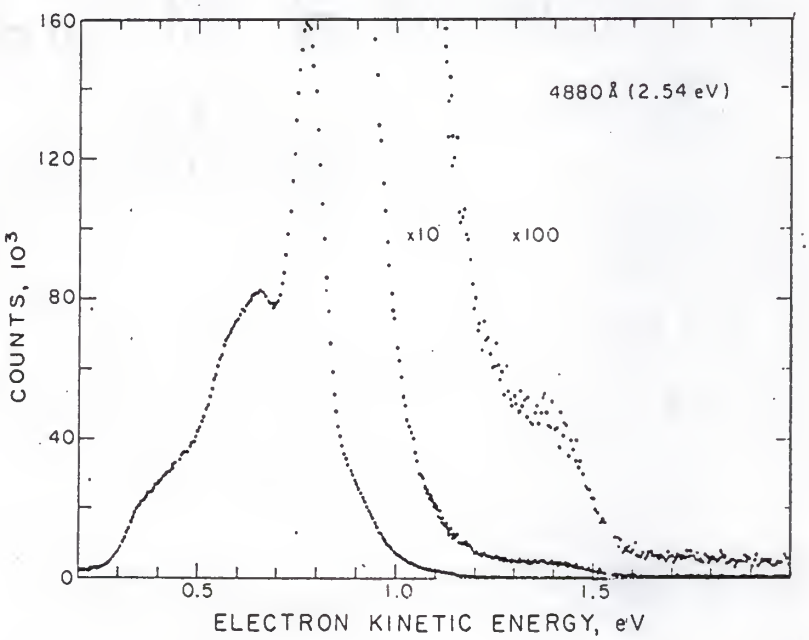

Figure 11. PES spectrum of $\underline{c}$-$C_5H_5^-$.

spectrum showed a large peak at ≈ 0.77 eV. When this energy was combined with photon energy (from an intracavity photon beam of an argon ion laser operated at 488.0 nm (2.540 eV)), the transition was 1.786 ± 0.020 eV. The fact that this peak dominated the PES spectrum suggested that it was the 0 ← 0 transition. The absence of progressions in ν' suggested that the main band was the large 0 ← 0

transition and that the geometry change between the anion and the neutral radical was small.

Since $\underline{c}$-$C_5H_5\bullet$ has D_{5h} symmetry, the Jahn-Teller distortion will result in one of the carbon atoms either being pushed inward or outward from the center of the molecule. The symmetry then allows for this distortion to be a linear combination of the Jahn-Teller distorted geometries, which allows the distortion to move around the molecule. This distortion has been examined by electron paramagnetic resonance (EPR).[65,66] The EPR studies in matrices conducted at 30 to 70 K indicated that this conclusion was correct and that the five hydrogens were equivalent. At low temperature (12 K), the hydrogens begin to "freeze out". If the Jahn-Teller distortion had a low activation barrier, the EPR should show no "frozen out" structures. It was observed that the critical, or transition temperature was dependent upon the matrix environment. With the radical frozen in a matrix of cyclopentadiene, the critical temperature was > 70 K. With neon as the host matrix, the critical temperature was 12 K. Noting that cyclopentadiene was a strongly orienting crystal, while neon was a weakly orienting crystal, the freezing out of the distortion is reasonable due to the ability of the matrix to hold the radical geometrically fixed and showed that the freezing out of a single structure was due largely to the matrix and not to an intrinsic effect. Thus the barrier to isomer interconversion was small.

In an attempt to determine if the resonant peaks could occur from some other states, Lineberger, et al.[51], noted that a partial assignment of the vibrations, taken from the IR spectrum obtained by

Heydaya and co-workers,[69] had been made by Purins and Feeley.[67] In the IR spectrum a splitting of the absorption lines by 300 cm^{-1} was observed. The splitting decreased to 220 cm^{-1} in $C_5D_5\bullet$ which indicated that a C-H vibration was involved in the absorption.

There were two possibilities for the 300 cm^{-1} splitting. The first would be if the splitting occurred in the radical ground electronic state. If the ground state was split, the higher level should be resolved at low vibrational populations. This possibility was eliminated due to the observed splitting in the low temperature ESR studies.[68] This leaves only one possibility, a distortion of the upper electronic state of $c\text{-}C_5H_5\bullet$. This distortion leads to a separation of vibrational states by about 300 cm^{-1}.

We might expect to see fine structure, or a strong $0 \leftarrow 0$ transition, in our experiment if the upper state is bound. This proved not to be the case. The EPD spectrum of $\underline{c}\text{-}C_5H_5^-$ is shown in Figure 12.[69] It can be seen that the EPD cross section rises slowly from the base line with no structure. The point where the cross section falls to zero at 707 ± 3 nm (1.753 ± 0.007 eV) is in excellent agreement with $EA(c\text{-}C_5H_5)$ = 1.786 ± 0.020 eV found previously.[51] To determine the EA of the $\underline{c}\text{-}C_5H_5\bullet$ the curve was fit using the threshold law, the first 30 nm (670 to 700 nm) were used to fit the data as described in Section I.C. and gave excellent agreement to the previous values.

Several concerns must be mentioned. The first is the presence or absence of hot band in the EPD spectrum. In Lineberger's apparatus, the $\underline{c}\text{-}C_5H_5^-$ ions were made by dissociative electron attachment with

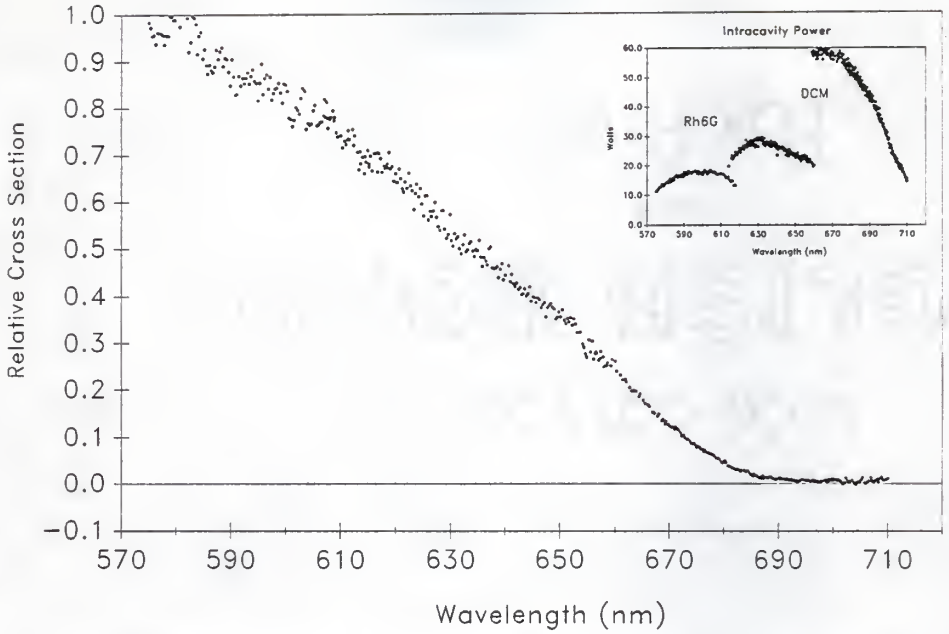

Figure 12. Relative EPD spectrum for $\underline{c}$-$C_5H_5^-$ in the FA (resolution 0.25 nm fwhm).

either ferrocene or cyclopentadiene. These ions were extracted from the source region, accelerated, mass selected, and injected into the photon beam interaction region. All these process were carried out at low pressures and vibrational quenching by collisions with a bath gas did not occur. The intensity of these vibrational excited state resonances are extremely weak in the PES spectrum and should not be observed in the FA/laser system, which was designed to produce thermalized ions.

Lineberger observed several peaks at 900 ± 100 cm^{-1} and 3300 ± 100 cm^{-1} above threshold in the PES spectrum which were assigned as a symmetric C-H stretch and the symmetric ring breathing mode.[70,71] These would occur at 648.5 ± 4 nm and 564.8 ± 5 nm, respectively. The

ring breathing mode would not be included in the present wavelength range utilized by the FA/laser EPD experiment. The C-H stretch is within the laser wavelength range, used but no evidence of this resonance is apparent.

To improve the ability to identify features in the FA/laser spectrum the experimental data was fit to a cubic spline then the derivative of this function was taken.[38,39] In the case of several alkoxyl anions (whose PED spectrum was determined by ICR/laser techniques) this method proved to be effective in identifying individual vibronic transitions.[72,73] In the $\underline{c}$-$C_5H_5^-$ spectrum these transitions were not seen.

I.E.3. Determination and Interpretation of the Electron Photodetachment Spectrum of Cyclopentadienylidene Anion Radical.

The species of primary interest in this investigation was $\underline{c}$-$C_5H_4^{\bullet -}$. This ion was first generated by McDonald,[12] et al. in 1980. The EPD spectra is shown in Figure 13. The experiments were conducted as previously described in section I.C.. The dyes used in this set of studies were Rhodamine 110 (545 to 605 nm), Rhodamine 6G (570 to 640 nm), and DCM (600 to 720 nm). The spectra followed the slowly rising integral cross section similar to that of the $\underline{c}$-$C_5H_5^-$ (Figure 12). The EPD spectrum was fit to the threshold law from 680 to 720 nm and yielded a calculated threshold value of 715.05 nm (39.97 kcal mol^{-1}). However, the observed threshold was at the wavelength at which the cross section becomes zero is 708 ± 3 nm. This is the value (708 nm) used in all calculations due to the objective nature of the threshold fit. The value for EA($\underline{c}$-C_5H_4) is, therefore,

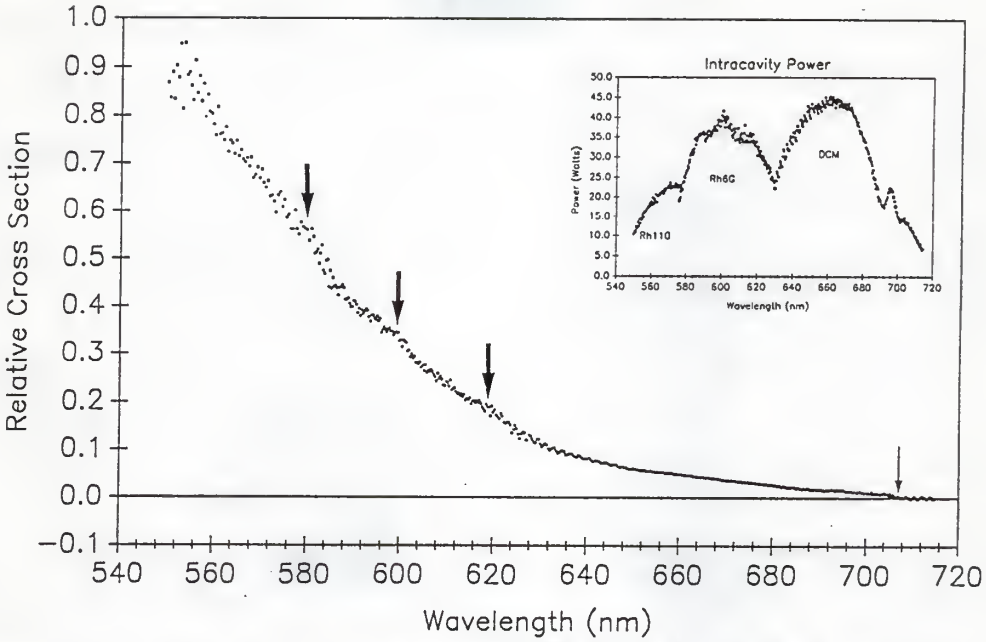

Figure 13. EPD spectrum of $\underline{c}$-$C_5H_4^{\bullet -}$. Inset shows intracavity photon beam power (watts). Spacing of experimental is 0.3 nm. The large arrows indicate onset of transitions to excited electronic state EPD onsets. The small arrow shows the 0 ← 0 EPD threshold.

40.37 ± 0.16 kcal mol^{-1}.

To determine if excited states could be observed the derivative of the photodetachment cross section was taken (Figure 14) as described in Section I.C.. The second derivative (Figure 15) was also used to identify the center of these peaks. The two (and possibly three) transitions became apparent by the use of these techniques. Smoothing of the EPD spectrum also enhanced the observation of the electronic transitions (Figure 16). Two clearly identifiable plateaus centered at 598 ± 3 nm (47.8 ± 0.2 kcal mol^{-1}) and 619 ± 3 nm (46.2 ± 0.2 kcal mol^{-1}) are observed (also see Figure 16). Another possible plateau was

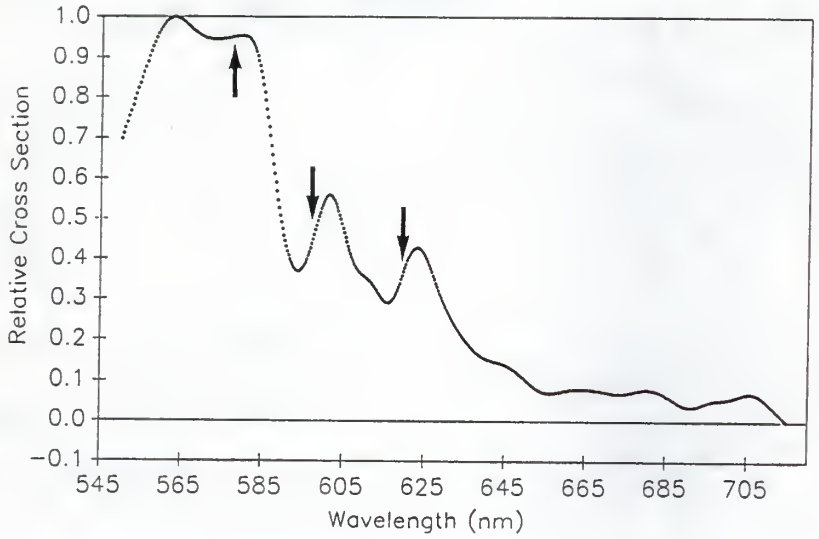

Figure 14. First derivative of $\underline{c}$-$C_5H_4^{\bullet -}$ EPD cross section. The spectrum shows the three electronic transitions.

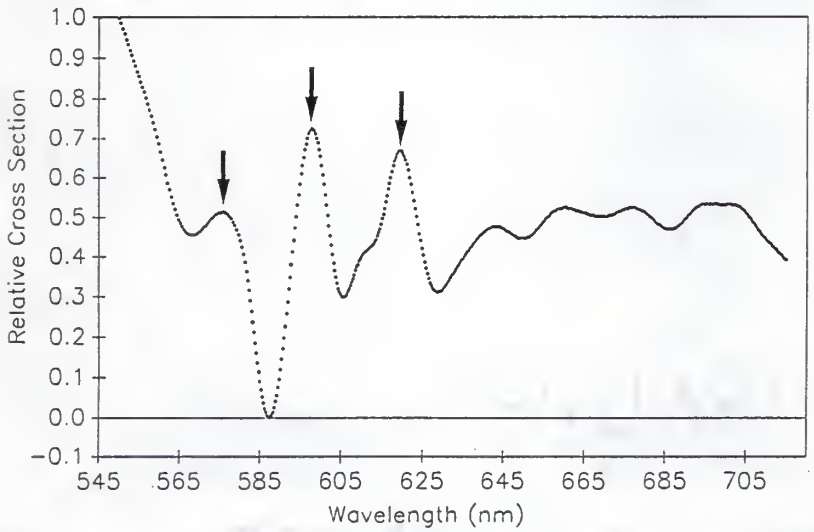

Figure 15. Second derivative of $\underline{c}$-$C_5H_4^{\bullet -}$ EPD cross section.

observed at 576.0 ± 3 nm (9.3 ± 0.2 kcal mol^{-1}) above threshold.

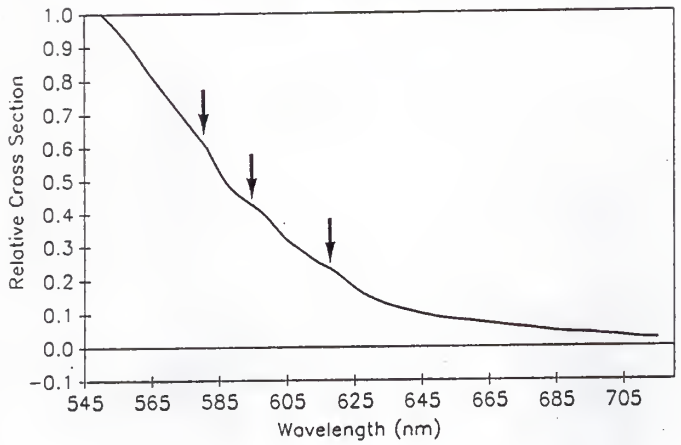

Figure 16. Smoothed EPD spectrum of $\underline{c}$-$C_5H_4^{\bullet -}$.

Since the plateaus are ≈ 10 nm wide and the energy spacing is large, it seems unlikely that they are vibrational or rotational in nature and must represent electronic transitions.

Recent calculations showed that the $^3B_1$ triplet was the carbene ground state[74], which agreed with prior ESR studies.[75] These calculations were based upon perturbation molecular orbital theory which treated the carbene as the union of a methylene and a polyene with 4n π-electron system. "This combination would favor the triplet ($^3B_1$) ground state."[79] The triplet state of the carbene has the $\sigma^1\pi^1$ electronic configuration. Both MNDO and SCF/6-31G* calculations show that the ground state of $^3B_1$ is a potential energy minimum. Some consideration was given to the singlet $\sigma^0\pi^2$ electronic configuration, since it would possess six π-electrons and be aromatic. However, the MNDO calculations showed that the ring could possibly deform and the resulting energy would be above that of the $^3B_1$ ground state.

These same calculations provided information on several excited states of $\underline{c}$-C_5H_4. At the CISD 6-31G* level, the first excited state was the singlet $^1A_2$ state which was only 7.3 kcal mol^{-1} above the ground state, which was assigned to the transition at 619 ± 3 nm in Figure 12. The transition at 598 ± 3 nm was assigned to the triplet $^3A_2$ state of $\underline{c}$-C_5H_4, which was calculated to be 8.3 kcal mol^{-1} above the ground state. The much weaker transition at 576 ± 3 nm in Figure 12 is tentatively assigned to the $^1A'$ state of c-C_5H_4 which is calculated to be 12.2 kcal mol^{-1} above the ground state.[78] The lower intensity for the latter transition was consistent with the calculated structure of the $^1A'$ state distorted from the planar C_{2v} geometry of the ground state to that of the nonplanar C_s geometry. This distortion occurs as a result of a out-of-plane bend of the carbenic carbon center. This would result in poor Frank-Condon overlap which reduces the probability for this EPD transition.

While the absolute energies calculated for such a complex molecule as $\underline{c}$-$C_5H_4(^3B_1)$ and its excited states would be suspect, the energy differences between the states of $\underline{c}$-C_5H_4 should be good. The experimental and calculated values are summarized in Table 3. The agreement in two values for $\delta\Delta\underline{H}_f^\circ$ is considered to be good.

The value of EA($\underline{c}$-C_5H_4) is also consistent with the expectation that EA($\underline{c}$-C_5H_4) ≈ EA($\underline{c}$-C_5H_5); the difference > 1 kcal mol^{-1}. This means that the energy difference between $\underline{c}$-$C_5H_4^{\bullet -}$ and $\underline{c}$-$C_5H_4(^3B_1)$ + e^-, and $\underline{c}$-$C_5H_5^-$ and $\underline{c}$-C_5H_5 + e^- are the same, although the absolute ($\Delta\underline{H}_f^\circ$) of all four species are different. It is, therefore, the relative

energy of the π-MO which detaches the e^- in the two systems that must be similar.

The proton affinity (PA) of a negative ion B^- is the negative of the enthalpy change for eq. 15. If B^- is allowed to react with HA

$$B^- + HA \rightarrow B + A^- \qquad (15)$$

$$-\Delta H^\circ_{rxn} = PA(B)$$

molecules of known gas phase acidity, the $PA(B^-)$ can be determined by the bracketing method. If there is no reaction, $PA(B^-) < PA(A^-)$; conversely, if proton transfer occurs $PA(B^-) > PA(A^-)$. By studing a number of different HA molecules the $PA(B^-)$ is bracketed. This method is similar to that used in EA bracketing studies described in section I.A.1. Using this method, the $PA(\underline{c}\text{-}C_5H_4^{\bullet -})$ was determined to be 379.3 ± 3.9 kcal mol^{-1}.[14,76] The $\Delta\underline{H}^\circ_{f,298}(\underline{c}\text{-}C_5H_4^{\bullet -})$ is calculated by eq. 16.

$$\Delta\underline{H}^\circ_{f,298}(\underline{c}\text{-}C_5H_4^{\bullet -}) = PA(\underline{c}\text{-}C_5H_4^{\bullet -}) + \Delta\underline{H}^\circ_{f,298}(\underline{c}\text{-}C_5H_5\bullet) - \Delta\underline{H}^\circ_{f,298}(H^+) \qquad (16)$$

Since both $\Delta\underline{H}^\circ_{f,298}(H^+)$ (368.6 kcal mol^{-1})[77] and $\Delta\underline{H}^\circ_{f,298}(\underline{c}\text{-}C_5H_5\bullet)$ (60.9 ± 1.2 kcal mol^{-1})[78] are known the only value required is the $PA(\underline{c}\text{-}C_5H_4^{\bullet -}) = \Delta\underline{H}^\circ_{acid}(c\text{-}C_5H_5\bullet)$. The value for the $\Delta\underline{H}^\circ_{f,298}(\underline{c}\text{-}C_5H_4^{\bullet -})$ is calculated to be 71.6 ± 3.2 kcal mol^{-1}. Because the threshold for EPD defined for a 0 K transition, the $\Delta\underline{H}^\circ_{f,298}$ must be corrected to $\Delta\underline{H}^\circ_{f,0}$. This is accomplished by subtracting the heat content $(H_t - H_0)$ of benzene (a compund that should possess a very similar heat content to that of $\underline{c}\text{-}C_5H_4^{\bullet -}$) and adding the heat content for the elements of

carbon and hydrogen in their standard states from the heat of formation of $\underline{c}\text{-}C_5H_4^{\bullet -}$ at 298 K. This is shown in eq. 17.

$$\Delta\underline{H}^{\circ}_{f,0}(\underline{c}\text{-}C_5H_4^{\bullet -}) = \Delta\underline{H}^{\circ}_{f,298}(\underline{c}\text{-}C_5H_4^{\bullet -})_{298} - (H_t - H_0)_{C_6H_6} + [3(H_t - H_0)_{H_2} + 6(H_t - H_0)_C] \quad (17)$$

The values for $(H_t - H_0)_{H_2}$ and $(H_t - H_0)_C$ are 0.25 kcal mole^{-1} and 2.02 kcal mole^{-1},[79] respectively. The value of $(H_t - H_0)_{C_6H_6}$ is 3.415 kcal mole^{-1}.[80] This calculation yields a value for $\Delta\underline{H}^{\circ}_{f,0}(\underline{c}\text{-}C_5H_4^{\bullet -})$ = 75.8 kcal mole^{-1}. Since the relative energies of the first three excited electronic states have been determined their $\Delta\underline{H}^{\circ}_f$ can be calculated by adding the EPD threshold energies to the ground state $\Delta\underline{H}^{\circ}_{f,0}$ (= 116.2 kcal mol^{-1}). The $\Delta\underline{H}^{\circ}_{f,0}(\underline{c}\text{-}C_5H_5(^1A_2))$ is calculated to be 122.1 ± 3.4 kcal mol^{-1}, $\Delta\underline{H}^{\circ}_{f,0}(c\text{-}C_5H_5^{\bullet -}(^3A_2))$ is calculated to be 123.7 ± 3.4 kcal mol^{-1}, and the $\Delta\underline{H}^{\circ}_{f,0}(c\text{-}C_5H_5^{\bullet -}(^1A'))$ is calculated to be 125.5 ± 3.4 kcal mol^{-1}. These corrections account for changes in the Boltzman distribution between the anion and the neutral, however, the differences between the distribution is small and the $\Delta\underline{H}^{\circ}_{f,298}(\underline{c}\text{-}C_5H_4)$ can be calculated by directly adding the threshold energies to the $\Delta\underline{H}^{\circ}_{f,298}(c\text{-}C_5H_4^{\bullet -})$. The $\Delta\underline{H}^{\circ}_{f,298}(\underline{c}\text{-}C_5H_5(^1A_2))$ is calculated to be 117.9 ± 3.4 kcal mol^{-1}, $\Delta\underline{H}^{\circ}_{f,298}(c\text{-}C_5H_5^{\bullet -}(^3A_2))$ is calculated to be 119.5 ± 3.4 kcal mol^{-1}, and the $\Delta\underline{H}^{\circ}_{f,298}(c\text{-}C_5H_5^{\bullet -}(^1A'))$ is calculated to be 121.3 ± 3.4 kcal mol^{-1}. These values have been summerized in table 2.

Another thermodynamic quantity of interest that can be derived from the experimental results is the bond dissociation energy of C-H bond in $\underline{c}\text{-}C_5H_5\bullet$ ($D^{\circ}(\underline{c}\text{-}C_5H_4^{\bullet}\text{-}H)$). It can be calculated using the thermodynamic cycle shown in Scheme 1. Specifically $\underline{D}^{\circ}(C_5H_4^{\bullet}\text{-}H)$ can

Table 3. Energetics of the Electronic States of $\underline{c}$-C_5H_4

State	λ	Energy	ΔE $=\delta\Delta H^\circ_{f,0} = \delta\Delta H^\circ_{f,298}$	$\Delta\underline{H}^\circ_{f,0}$ [a]	$\Delta\underline{H}^\circ_{f,298}$	Calculated Energy[b] Difference
$\underline{c}$-$C_5H_4(^3B_1)$	708	40.37	0.0	116.1	112.0	0.0
$\underline{c}$-$C_5H_4(^1A_2)$	619	46.20	5.83	122.0	117.8	7.3
$\underline{c}$-$C_5H_4(^3A_2)$	598	47.80	7.43	123.6	119.4	8.4
$\underline{c}$-$C_5H_4(^1A')$	576	49.60	9.23	125.4	121.2	12.2

[a]See text for discussion. [b]See Ref. 74.

be calculated by eq. 18.

Since $\Delta H^{\circ}_{acid}(\underline{c}\text{-}C_5H_5\bullet) = PA(\underline{c}\text{-}C_5H_4^{\bullet -})$, eq. 18 is transformed into eq. 19. In eq. 19, IP(H•) = 313.6 kcal mol^{-1}[181] and the $PA(\underline{c}\text{-}C_5H_4^{\bullet -})$ = 379.3 ± 3.2 kcal mol^{-1};[14] and $EA(\underline{c}\text{-}C_5H_4^{\bullet -})$ = 40.37 ± 0.16 kcal mol^{-1}. This leads to $\underline{D}^{\circ}(\underline{c}\text{-}C_5H_4^{\bullet}\text{-}H)$ = 106.1 ± 3.4 kcal mol^{-1}. A related value

Scheme 1.

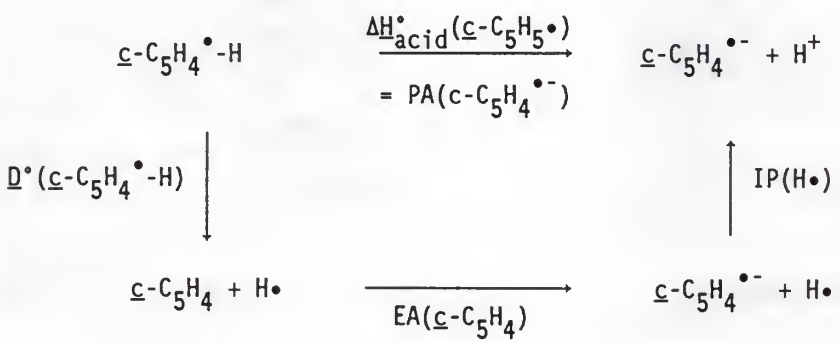

$$\underline{D}^{\circ}(C_5H_4^{\bullet}\text{-}H) = EA(c\text{-}C_5H_4) + IP(H\bullet) - \Delta H^{\circ}_{acid}(\underline{c}\text{-}C_5H_5\bullet) \qquad (18)$$

$$\underline{D}^{\circ}(\underline{c}\text{-}C_5H_4^{\bullet}\text{-}H) = EA(\underline{c}\text{-}C_5H_4^{\bullet -}) + IP(H\bullet) - PA(\underline{c}\text{-}C_5H_4^{\bullet -}) \qquad (19)$$

is the C-H bond dissociation energy of cyclopentadienyl anion, $\underline{D}^{\circ}(\underline{c}\text{-}C_5H_4\text{-}H^-)$ = 104 ± 5 kcal mol^{-1}.[12] Therefore, the C-H bond energies in $c\text{-}C_5H_5\bullet$ and $c\text{-}C_5H_5^-$ are not affected by the addition or loss of an electron in the highest occupied π-molecular orbital.

Appendix. Ligand Substitution Reactions of $(OC)_3Fe^{\bullet -}$ with ^{13}CO.

The ligand substitution reactions of 17-electron organometallic negative ion species have been extensively studied.[82,83] The purpose of the study of the reactions of reactions of $(OC)_3Fe^{\bullet -}$ with CO and ^{13}CO was to determine the competitive rate constants for the exchange of CO ligands and the assumed termolecular addition of CO forming $(OC)_4Fe^{\bullet -}$. While the exchange of CO ligands is thermoneutral, the addition reaction is exothermic and requires collisional stabilization of the vibrationally excited adduct $[(OC)_4Fe^{\bullet -}]^*$ with the helium buffer gas.

The reactions of $(OC)_3Fe^{\bullet -}$ with CO and ^{13}CO were carried out in the FA (Figure 3). A fast flow of helium buffer gas ($\bar{v}$ at 298 K = 80 m/s) was established in the 1.5 meter long flow tube by a large, fast pumping Roots blower/mechanical pump. Ions were generated by dissociative electron attachment on $Fe(CO)_5$. The electron gun used was constructed of a rhenium filament and a tungsten accelerating grid. Electrons were generated by passing a current (10 A) through the filament while holding it at a high negative potential (-200 V). The electron guns emission current was measured to be 1 to 2 mA. The electrons mixture of $(OC)_{3,4}Fe^{\bullet -}$ ions were cooled to their ground states with the helium buffer gas. The CO and ^{13}CO, stored in gas bulbs were added via the neutral inlet. The ion/helium flow was sampled via 1 mm orifices in two molybdenum nose cones into the differentially pumped compartment containing a quadupole mass filter and and electron multiplier, which continuously samples the ion composition of the flow.

The inlet for CO and ^{13}CO is located downstream from the ion production region. The distance (time) for the pseudo-first order (CO and ^{13}CO is in large excess) ion/molecule reaction is known and held constant as varing amounts of CO or ^{13}CO are added to the flow. The ion intensities of $(OC)_3Fe^{\bullet -}$ and product signals are recorded at each neutral concentration. From the plot of $\log((OC)_3Fe^{\bullet -})$ vs. CO or ^{13}CO concentration the slope is determined and converted into the bimolecular rate constant for the reaction between $(OC)_3Fe^{\bullet -}$ + CO or ^{13}CO. This conversions has been described in detail elsewhere.[12]

The ions, $(OC)_3Fe^{\bullet -}$ and $(OC)_4Fe^{\bullet -}$, are made by dissociative electron attachment of $Fe(CO)_5$. This process produced a mixture of $(OC)_4Fe^{\bullet -}$ (m/z 168) and $(OC)_3Fe^{\bullet -}$ (m/z 140). The reaction of $(OC)_4Fe^{\bullet -}$ with CO was shown not to occur ($k < 10^{-13}$ cm^3 molecule^{-1} sec^{-1}).

Loading of glass storage bulbs with CO was made from an aluminum cylinder that had been specially purchased (Matheson). The labeled ^{13}CO (MSD Isotopes; purity 99.8%) was obtained in a glass bulb. Two independent storage bulbs were used in the study to detect errors in bulb loadings. Storage bulbs were loaded with 15 to 30 torr CO (or ^{13}CO) and diluted to a 5 to 10% concentration with helium.

The reaction of the 15-electron complex $(OC)_3Fe^{\bullet -}$ (m/z 140) with CO exclusively produced $(OC)_4Fe^{\bullet -}$ (m/z 168) with the kinetic data given in Table A1. The apparent bimolecular rate constant, k_{app} = 1.4 x 10^{-10} cm^3 molecule^{-1} sec^{-1}, was in good agreement with that previously reported for this reaction (k_{app} = 1.6 x 10^{-10} cm^3 molecule^{-1} sec^{-1}.[85]

The corresponding reaction of $(OC)_3Fe^{\bullet -}$ with ^{13}CO should not only give the addition product, but also reveal the CO ligand substitution

channel forming $(OC)_2(O^{13}C)Fe^{\bullet -}$ at m/z 141 (Figure A1). To determine the branching fractions for the addition and substitution channels in Figure A1 as accurately as possible, the percent conversion of $(OC)_3Fe^{\bullet -}$ to product ions must be large so that the

Table A1. Summary of Kinetic and Product Data for the reaction of $(OC)_3Fe^{\bullet -}$ with CO.

Rxn. No.	P_{He}	Product Ion	k_{app}, [a] cm^3 $molecule^{-1}$ sec^{-1}
1	1.0	$(OC)_4Fe^{\bullet -}$	1.4×10^{-10}
2	1.0	$(OC)_4Fe^{\bullet -}$	1.4×10^{-10}
Avg.			1.4×10^{-10}

[a]This is the apparent bimolecular rate constant for what is assumed to be a termolecular reaction.

product ion signal intensities are large. This high percent conversion of $(OC)_3Fe^{\bullet -}$ requires a relatively large concentration of ^{13}CO to be added to the flow. This requirment means that secondary reactions of the coordinatively and electronically unsaturated primary substitution product $(OC)_2(O^{13}C)Fe^{\bullet -}$ will occur. The sequntial production of the observed product ions is shown in Scheme A1. The starting and product ions in Scheme A1 fall into two grops at m/z 140 to 143 and 168 to 172.

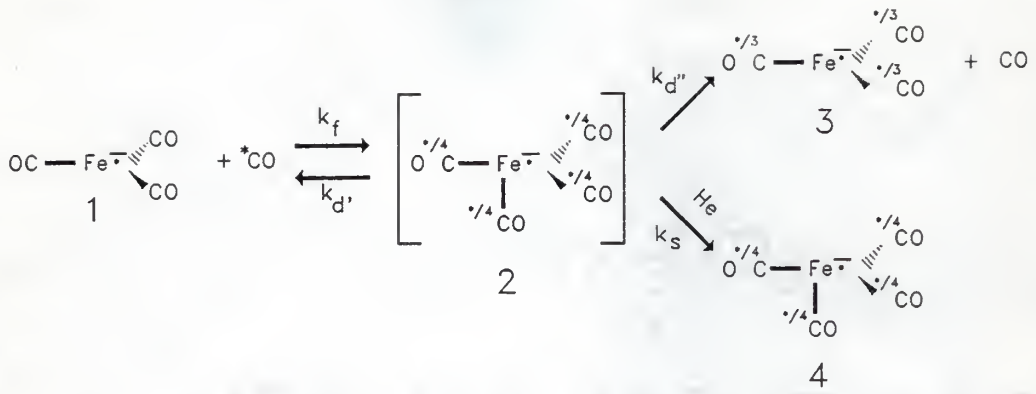

Figure A1. Mechanism of ligand addition and substitution $(OC)_3Fe^{\bullet-}$ with ^{13}CO (= $^{*}CO$).

Scheme A1.

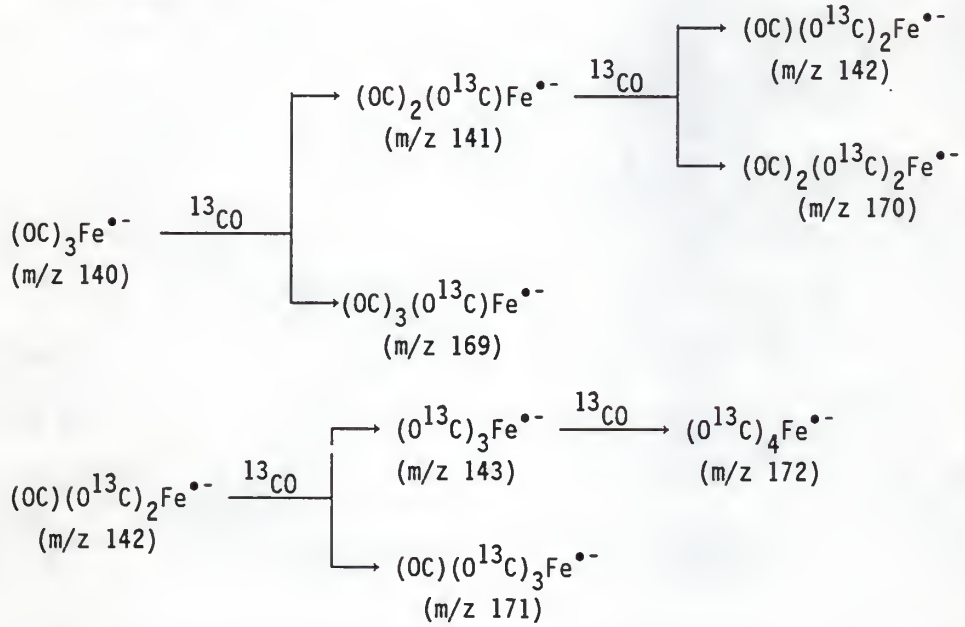

This fact required that the quadupole mass spectrometer be operated at ≥ unit mass resolution. It was assumed that mass discrimination was not present over this 33 amu range.

Of the products in Scheme A1, $(OC)_3(O^{13}C)Fe^{\bullet -}$ (m/z 169) is unique in that it is the only primary ion product of the addition channel (Figure A1). The remaining product ions at m/z 141 to 143 and 170 to 172 are derived from the primary CO ligand substitution channel Figure A1. Therefore, the data analysis of the integrated ion intensities contributing to the two primary product forming channels was treated as shown in Table A2.

Table A2. Isotopically Labled Ions Formed in the Reaction of $(OC)_2Fe^{\bullet -}$ with ^{13}CO and their Involvement in the Substitution and Addition Channels.

Labeled Ion Arising from the Addition Channel	Labeled Ions Arising from the Substitution Channel
$(OC)_3(O^{13}C)Fe^{\bullet -}$ (m/z 169)	$(OC)_2(O^{13}C)Fe^{\bullet -}$ (m/z 141)
	$(OC)(O^{13}C)_2Fe^{\bullet -}$ (m/z 142)
	$(O^{13}C)_3Fe^{\bullet -}$ (m/z 143)
	$(OC)_2(O^{13}C)_2Fe^{\bullet -}$ (m/z 170)
	$(OC)(O^{13}C)_3Fe^{\bullet -}$ (m/z 171)
	$(O^{13}C)_4Fe^{\bullet -}$ (m/z 172)

A further problem in the analysis of the data was the naturally occuring isotopes of Fe ($^{54}Fe/^{56}Fe/^{57}Fe/^{58}Fe$ = 5.8%/91.8%/2.1%/0.3%), C ($^{12}C/^{13}C$ = 98.89%/1.11%)), and O ($^{16}O/^{18}O$ = 99.76%/0.20%) in these ions.[84] For $(OC)_3Fe^{\bullet -}$, the percentage of the normalized isotopes are (M-2) = 6.32%, (M) = 100%, (M+1) = 5.72%, and (M+2) = 0.95%, while for $(OC)_4Fe^{\bullet -}$ these percentages are (M-2) = 6.32%, (M) = 100%, (M+1) =

6.85%, (M+2) = 1.13%. To obtain the true integral value of the ion at a unit mass, the measured integral for that mass peak in the negative ion mass spectrum must be corrected for all contributions of isotopes of ions at other nominal masses which contribute to that mass peak. For example, the amount of $(OC)_2(O^{13}C)Fe^{\bullet -}$ present in the intergral peak at m/z 141 is the (intergral value of m/z 141) - [((M+1) of $(OC)_3Fe^{\bullet -}$ at m/z 140) + ((M-2) of $(O^{13}C)_3Fe^{\bullet -}$ at m/z 143)]. Summing these corrected ion intergral values according to Table A2 yielded the branching fractions for the two product forming channels in Figure A1.

Figure A2 is three-dimensional mass spectrum of the reaction of $(OC)_3Fe^{\bullet -}$ with ^{13}CO. The axes in the plane of the plot are the relative intensity vs. m/z, while the axis perpendicular the the plane of the plot is increasing ^{13}CO concentration. The decay of $(OC)_3Fe^{\bullet -}$ (m/z 140) along with the growth of the product peaks at m/z 141 to 143 and 169 to 172 can be seen. A kinetic semi-log plot of log(ion intensity) vs. increasein ^{13}CO concentration can be seen in Figure. A3. The kinetics and products obtained from the reactions of $(OC)_3Fe^{\bullet -}$ with ^{13}CO are summerized in Table A3; the rate constants had correlation coefficients > 0.99. The reaction exhibited a slight pressure effect. As seen in Table A2, as the P_{He} increased the rate constant is effected only slightly while the branching fractions are effected to a larger degree. This is consistent with the assumption that the addition product is a termolecular reaction involving helium.

The reaction of $(OC)_3Fe^{\bullet -}$ with CO should proceed via the associative mechanism shown in Figure A1. This mechanism involves the addition of CO to a vacant coordination site in the metal complex.

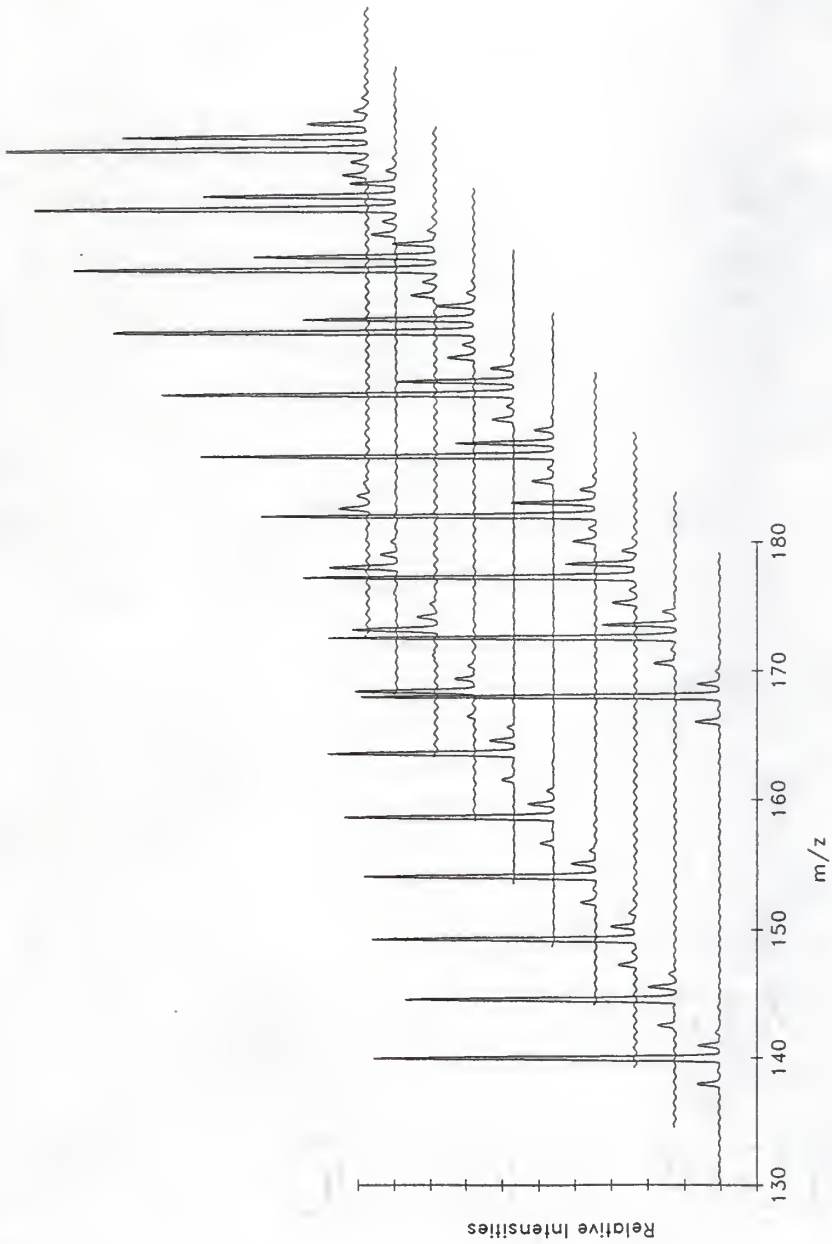

Figure A2. Three-dimensional mass spectral representation of the reaction of $(OC)_3Fe^{\bullet-}$ and ^{13}CO.

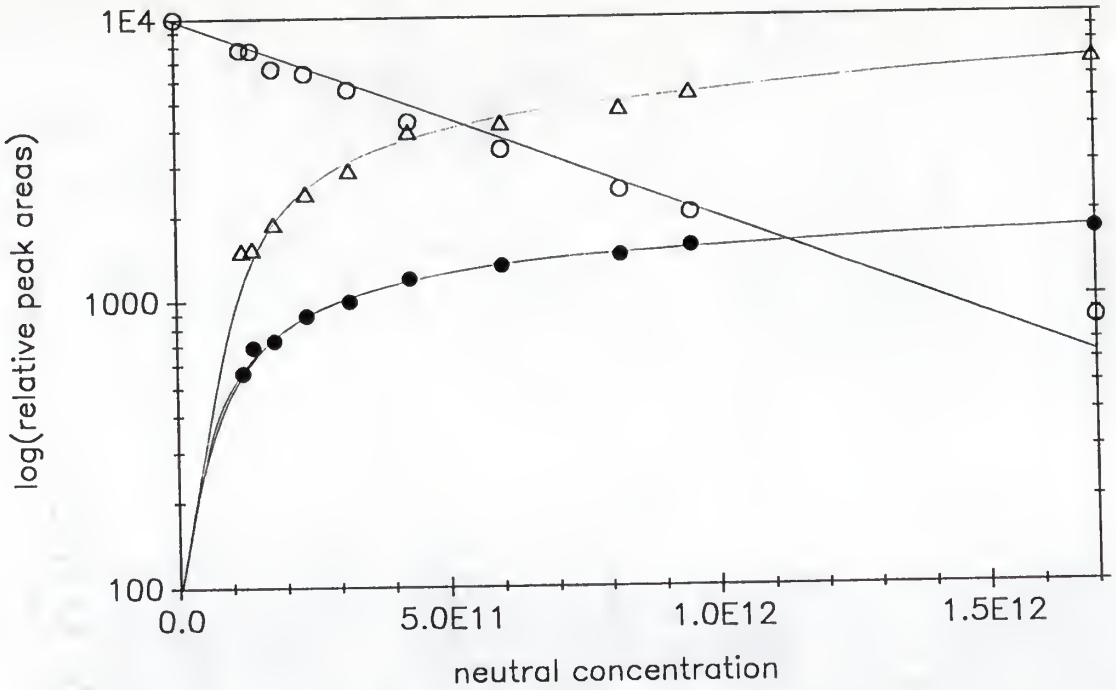

Figure A3. Kinetic semi-log plot for the reaction of $(OC)_3Fe^{\bullet -}$ and ^{13}CO. Open circles represent $(OC)_3Fe^{\bullet -}$ while the triangles and filled circles are the addition and substitution products, respectively.

Table A3. Summary of Kinetic and Product Data for the Reactions of $(OC)_3Fe^{\bullet-}$ with ^{13}CO.

Rxn. No.	P_{He}	Product Ions	Branching Fraction[a]	Rate Constants for Exchange/Addition[b]
1	1.1	$(OC)_2(O^{13}C)Fe^{\bullet-}$ + $(OC)(O^{13}C)_2Fe^{\bullet-}$ + $(O^{13}C)_3Fe^{\bullet-}$ + $(OC)_2(O^{13}C)_2Fe^{\bullet-}$ + $(OC)(O^{13}C)_3Fe^{\bullet-}$ + $(O^{13}C)_4Fe^{\bullet-}$ (m/z 141, 142, 143, 170, 171, 172)	0.26	$k_{exc} = 5.5 \times 10^{-11}$[c]
		$(OC)_3(O^{13}C)Fe^{\bullet-}$ (m/z 169)	0.74	$k_{add} = 1.6 \times 10^{-10}$[c]
2	1.0	$(OC)_2(O^{13}C)Fe^{\bullet-}$ + $(OC)(O^{13}C)_2Fe^{\bullet-}$ + $(O^{13}C)_3Fe^{\bullet-}$ + $(OC)_2(O^{13}C)_2Fe^{\bullet-}$ + $(OC)(O^{13}C)_3Fe^{\bullet-}$ + $(O^{13}C)_4Fe^{\bullet-}$ (m/z 141, 142, 143, 170, 171, 172)	0.28	$k_{exc} = 5.3 \times 10^{-11}$[d]
		$(OC)_3(O^{13}C)Fe^{\bullet-}$ (m/z 169)	0.72	$k_{add} = 1.4 \times 10^{-10}$[d]

Table A3, (continued)

AVERAGE			0.27 ± 0.01	$k_{exc} = 6.5 \times 10^{-11}$ [e]
			0.73 ± 0.01	$k_{add} = 1.6 \times 10^{-10}$ [e]
3	0.7	$(OC)_2(O^{13}C)Fe^{\bullet-}$ + $(OC)(O^{13}C)_2Fe^{\bullet-}$ + $(O^{13}C)_3Fe^{\bullet-}$ + $(OC)_2(O^{13}C)_2Fe^{\bullet-}$ + $(OC)(O^{13}C)_3Fe^{\bullet-}$ + $(O^{13}C)_4Fe^{\bullet-}$ (m/z 141, 142, 143, 170, 171, 172)	0.34	$k_{exc} = 8.8 \times 10^{-11}$ [e]
		$(OC)_3(O^{13}C)Fe^{\bullet-}$ (m/z 169)	0.66	$k_{add} = 1.7 \times 10^{-10}$ [e]

[a]Errors in these individual branching fractions are considered to be ±5% absolute from the average values given and are the averages of the neutral concentration branching fractions. [b]k_{exc}'s and k_{add}'s are in cm^3 $molecule^{-1}$ sec^{-1}. [c]Calculated from $k_{total} = 2.1 \times 10^{-10}$ cm^3 $molecules^{-1}$ sec^{-1}. [d]Calculated from $k_{total} = 1.9 \times 10^{-10}$ cm^3 $molecules^{-1}$ sec^{-1}. [e]Calculated from $k_{total} = 2.6 \times 10^{-10}$ cm^3 $molecules^{-1}$ sec^{-1}.

Because calculations showed that $(OC)_3Fe$ possesses C_{3v} symmetry,[85] $(OC)_3Fe^{\bullet -}$ is expected to possess a similar geometry which is only slightly bent from trigonal planar geometry with the electron density above the plane of the ligands. The results of Breeze, Burdett, and Turner[86] established the trigonal pyramidal geometry for $(OC)_4Fe^{\bullet -}$ with C_{3v} symmetry. Coordination of the CO molecule from either the top or bottom face of the nearly planar $(OC)_3Fe^{\bullet -}$ ion would directly yield the trigonal pyramid structure of $(OC)_4Fe^{\bullet -}$.

Coordination of ^{13}CO to $(OC)_3Fe^{\bullet -}$ should yield excited $(OC)_3Fe^{\bullet -}$ initially with the ^{13}CO ligand in the axial site of the trigonal pyramid structure. Since the scrambling of the labeled ^{13}CO ligand is likely to occur in the timeframe of molecular vibrations ($\approx 10^{-13}$ sec) compared to the much longer lifetime of the excited complex, the first product ion **2** is shown in Figure A1 with the complete lable scrambling. The scrambling mechanism could involve either a tetrahedral or square planar structure as a transition state or intermediate possibly related to a Berry pseudo-rotation. Dissociation of **2** would by the microscopic reverse of the addition process with ejection of ^{13}CO by $k_{d'}$ and loss of CO by $k_{d''}$; these rate constants are related by $k_{d'} = 3k_{d''}$.

In the mechanism in Figure A1, the CO and ^{13}CO are rapidly equilibrated. The equilibrated species **2** can either (a) be stabilized by collisions with the helium buffer gas or (b) lose a CO (or the ^{13}CO) ligand to form $(OC)_2(O^{13}C)Fe^{\bullet -}$ (or $(OC)_3Fe^{\bullet -}$); in (b) only the former process can be observed. Two assumptions are made in the mechanism and kinetic analysis (a) 1 collision of $[(OC)_3(O^{13}CO)Fe^{\bullet -}]^*$ with a helium atom removes enough energy so that the loss of a ligand does not occur

(b) the rearrangment (scrambling of the ^{13}CO) is fast. Both assumption are resonable. If these two assumptions hold, limits of $k_{d'}$, $k_{d''}$, and $k_s[He]$ can be calculated.

By definition k_d is defined as the total rate constant for exchange, $k_d = k_{d'} + k_{d''}$. Once ^{13}CO had added to $(OC)_3Fe^{\bullet -}$ and label scrambling had occurred to yeild **2** (Figure A1) the probability for loss of CO vs. the ^{13}CO ligand is a ratio of 3:1, respectively. This statistical factor means that the branching fraction for the exchange reaction channel reported in Table A3 is 25% smaller than the real value. Thus, the total branching fraction for exchange (k_d) due to observed ($k_{d''}$) and unobserved echange ($k_{d'}$) increases to 0.34. Since the amount of addition is constant, the new fraction of 0.34/0.73 must be normilized to give the true branching fractions of 0.32 and 0.68 for exchange and addition, respectively.

The relationship between the ratio of the branching fractions of the processes in Figure A1 and the rate constants k_d and $k_s[He]$ is given in eq. A1. In eq. A1, the amount of each process is equal to the rate constant for the process divided by the sum of the rate constants for both processes. Equation A1 simplifies to eq. A2.

$$\frac{\text{exchange branching fraction}}{\text{addition branching fraction}} = \frac{\dfrac{k_d}{k_d + k_s[He]}}{\dfrac{k_s[He]}{k_d + k_s[He]}} = \frac{0.32}{0.68} \qquad \text{(A1)}$$

$$\frac{0.32}{0.68} = \frac{k_d}{k_s[He]} \qquad \text{(A2)}$$

The collision frequency $k_3[He]$ is arrived at in the following way. Langevin theory[87] was used in theis calulation where the neutral molecule (helium) was treated as an induced dipole calculated from its polarizability (0.203×10^{24} cm^3)[88] and the ion as a point charge (eq. A3). In eq. A3, q is the charge of the ion, α is the polarizability of the neutral molecule, and μ is the reduced mass. The calculated

$$k_{Lan} = 2\pi q(\alpha/\mu)^{1/2} \qquad (A3)$$

Langevin cross section was 7.5×10^{-10} cm^3 $atom^{-1}$ sec^{-1}. From the ideal gas law (eq. A4),[89] the concentration of the helium is calculated to be $[He] = 3.6 \times 10^{16}$ molecules cm^{-3}. In eq. 4, ρ is the

$$\rho = (P \times n \times 10^3 L/m^3)/(R \times T) \qquad (A4)$$

concentration of the gas, n is Avagadros number ($= 6.02 \times 10^{23}$ molecules mol^{-1}), V is the volume containing the gas, P is the pressure of the gas (= 1.1 torr = 1.463×10^{-3} Bar), R is the ideal gas constant (= 0.83144 L Bar K^{-1} mol^{-1}) at T is the temperature (= 298 K). Multiplying the Langevin cross section by [He] yields the collision frequency, 2.7×10^7 sec^{-1}, of the ions with the helium atoms at this pressure. This places a lowere limit on the lifetime of the excited $[(OC)_3(O^{13}C)Fe^{\bullet -}]^*$ ion of 3.7×10^{-8}, the reciprocal of the collision frequency.

Equation A2 was solved for a lower limit of $k_d = 1.3 \times 10^7$ sec, which yeilds $k_{d'} = 3.3 \times 10^6$ sec^{-1} and $k_{d''} = 9.8 \times 10^6$ sec^{-1} as lower limits.

1. (a) Freeman, G. R. Radiat. Res. Rev. **1968**, 1, 1. (b) Fehsenfeld, F. C.; Schmeltekopf, A. L. Schiff, H. I.; Ferguson, E. E. Planet. Space Sci. **1967**, 15, 373. (c) Leob, L. B. "Basic Process in Gaseous Electronics"; University of California: Los Angeles, 1961; p 375. (d) Lovelock, J. E. Nature (London) **1961**, 187, 49. (e) Lovelock, J. E. Anal. Chem. **1963**, 35, 474. (f) Wentworth, W. E.; Chen, E. C. M. J. Chromatogr. **1979**, 186, 99. (g) Wentworth, W. E.; Kao. L. W.; Backer, R. S. J. Phys. Chem. **1975**, 79, 1161. (h) Rich, P. R. Faraday Discuss. Chem. Soc. **1982**, 74, 3138. (i) Cristophorou, L. G. Adv. Electron. Electon. Phys. **1978**, 46, 55. (j) Szwarc, M. Prog. Phys. Org. Chem. **1968**, 6, 323. (k) Biergleb, G. Angew. Chem., Int. Ed. Engl **1964**, 3, 617. (l) Sutin, N. Prog. Inorg. Chem. **1983**, 30, 442.

2. (a) Hunt, D. F.; Stafford, G. C.; Crow, F. W.; Russel, J. W. Anal. Chem. **1976**, 48, 2098. (b) Buchanan, M. V.; Olerich, G. Anal. Chem. **1984**, 19, 486. (c) Iida, Y.; Daishima, S. Chem. Lett., **1983**, 273. (d) Harrison, A. G. "Chemical Ionization Mass Spectrometry"; CRC: Boca Raton, FL, 1984. (e) Clayton, E.; Wakefeild, A. J. J. Chem. Soc., Chem. Commun. **1984**, 969.

3. Eberson, l. Adv. Free Radical Biol. Med. **1975**, 1, 19.

4. Christodoulides, A. A.; McCorkle, D. L.; Christophorou, L. G. "Electron Molecule Interactions and Their Applications"; Academic: New York, 1984; Vol. 2.

5. (a) Kebarle, P. Annu. Rev. Phys. Chem. **1977**, 28, 495. (b) Grimsrud, E. P.; Chowdury, S.; Kebarle, P. Int. J. Mass Spectrom. Ion Processes **1986**, 68, 57.

6. (a) Brehm, B.; Gusinow, M. A.; Hall, J. L. Phys. Rev. Lett. **1967**, 19, 737. (b) Siegal, M. W.; Celotta, R. J.; Hall, J. L.; Levine, J.; Bennett. R. A. Phys. Rev. **1972**, A 6, 607. (c) Lepold, D. G.; Murray, K. K.; Stevens Miller, A. E.; Lineburger, W. C. J. Chem. Phys. **1985**, 83, 4849.

7. (a) Wetzel, D. M.; Brauman, J. I. Chem. Rev. **1987**, 87, 607. (b) Drzaic, P. S.; Brauman, J. I. J. Phys. Chem. **1984**, 88, 5285.

8. (a) McIver, R. T.; Fukuda, E. K. Lect. Notes Chem. **1982**, 164. (b) Fukuda, E. K.; McIver, R. T. J. Chem. Phys. **1982**, 77, 4942. (c) Fukuda, E. K.; McIver, R. T. J. Chem. Phys. **1983**, 87, 2993. (d) Fukuda, E. K.; McIver, R. T. J. Am. Chem. Soc. **1985**, 107, 2291.

9. Feshenfeld, F. C.; Ferguson, E. E.; Schmeltekopf, A. L. J. Chem. Phys. **1966**, 45, 1844.

10. Henglein, A.; Muccini, G. A. J. Chem. Phys. **1959**, 31, 1426.

11. (a) Hughes, B. M.; Lifshitz, C.; Teirnan, T. O. J. Chem. Phys., **1973**, 59, 3162. (b) Lifshitz, C.; Teirman, T. O.; Hughes, B. M. J. Chem. Phys. **1973**, 59, 3182. (c) Lifshitz, C. J. Chem. Phys. **1983**, 87, 3474.

12. McDonald, R. N.; Chowdury, A. K.; Setser, D. W. J. Am. Chem. Soc. **1980**, 102, 6491.

13. Bartmess, J., "The 1987 Gas Phase Acidity Scale," University of Tennessee.

14. Herbst, E.; Patterson, T. A.; Lineberger, W. C. J. Chem. Phys. **1974**, 61, 1300.

15. (a) Hogg, A. M.; Kebarle, P. J. Chem. Phys. **1965**, 43, 449. (b) Heinis, T.; Chowdury, S.; Kabarle, P. J. Am. Chem. Soc. **1986**, 108, 4662. (c) Kebarle, P. Annu. Rev. Phys. Chem. **1977**, 28, 495. (d) Grimsrud, E. P.; Chowdury, S.; Kebarle, P. J. Am. Chem. Soc. **1985**, 107, 4627. (d) Grimsrud, E. P.; Chowdury, S.; Kebarle, P. J. Chem. Phys. **1985**, 83, 1059. (e) Grimsrud, E. P.; Chowdury, S.; Kebarle, P. J. Chem. Phys. **1985**, 83, 3983. (f) Grimsrud, E. P.; Chowdury, S.; Kebarle, P. Int. J. Mass. Spectrom. Ion Processes **1986**, 68, 57. (g) Grimsrud, E. P.; Heinis, T.; Chowdury, S.; Kebarle, P. J. Phys. Chem. **1986**, 90, 2747. (h) Grimsrud, E. P.; Heinis, T.; Chowdury, S.; Kebarle, P. J. Am. Chem. Soc. **1986**, 108, 3630. (i) Nicol, G.; Chowdury, S.; Kebarle, P. Chem. Phys. Lett. **1986**, 127, 130. (j) Chowdury, S.; Kebarle, P. J. Am. Chem. Soc. **1986**, 108, 5453.

16. (a) Seigel, M. W.; Celotta, R. J.; Hall, J. L.; Bennett, R. A. Phys. Rev. **1972**, A 6, 607. (b) Mead, R. D.; Stevens, A. E.; Lineberger, W. C. In "Gas Phase Ion Chemistry"; Bowers, M. T., Ed.; Acedemic: New York, 1984 Vol. 3.

17. Seigel, M. W.; Celotta, R. J.; Hall, J. L.; Bennett, R. A. Levine, J. Phys. Rev. **1972**, A 6, 631.

18. (a) Leopold, D. G.; Murray, K. K.; Miller, S.; Lineberger, W. C. J. Chem. Phys. **1985**, 83, 4849. (b) Ellison, G. B.; Engelking, P. C.; Lineberger, W. C. J. Chem. Phys. **1982**, 86, 4873.

19. Ellis, H. B., Ellison, G. B. J. Chem. Phys. **1983**, 78, 6541.

20. Zetsch, C.; Stuhl, F. Chem. Phys. Lett. **1975**, 33, 375.

21. Celotta, R. J.; Bennett, R. A.; Hall, M. W.; Siegel, M. W.; Levine, R. D. J. Phys. Rev. , **1972**, A 6, 631.

22. (a) Kirmse, W. Carbene Chemistry Acedemic, New York, **1971**. (b) Carbenes, ed. Jones, M.; Moss, R. A., Ed. Wiley-Interscience, New York, **1975**, Vol. 2. (c) Lengel, R. K.; Zare, R. N. J. Am. Chem. Soc. **1978**, 100, 7495.

23. Gordon W. T.; Davidson, E. R. Annu. Rev. Phys. Chem. **1979**, 30, 125.

24. (a) Frey, H. M.; Kennedy, G. J. J. Chem. Soc. Chem. Commun. **1975**, 1975, 233. (b) Frey, H. M.; Kennedy, G. J. J.Chem. Soc. Faraday Trans. **1977**, 173, 164. (c) Hase, W. L.; Kelly, P. M. J. Chem. Phys. **1977**, 66, 5093.

25. (a) Montes, D. L.; Dietz, T. G.; Duncan, T. G.; Smalley, R. E. Chem. Phys. **1980**, 45, 133 (b) Danon, J.; Filseth, S. V.; Feldmann, D.; Zacharias, H.; Dugan, C. H.; Welge, K. H. Chem. Phys. **1978**, 29, 345. (c) Feldmann, D.; Zacharias, H.; Meier, K.; Welge, K. H. Chem. Phys. Lett. **1978**, 59, 171.

26. Zittel, P. F.; Ellison, G. B.; ONeil, S. V.; Herbst, E.; Lineberger, W. C. Reinhardt, W. P. J. Am. Chem. Soc. **1976**, 98, 3731.

27. (a) Brauman, J.I.; Wetzel, D. M. Chem. Rev, **1987**, 87, 607. (b) Zimmerman, A. H.; Brauman, J. I. J. Chem. Phys. **1977**, 66, 5823. (c) Zimmerman, A. H.; Reed, K. J.; Brauman, J. I. J. Am. Chem. Soc. **1977**, 99, 7203. (d) Jackson, R. L.; Zimmerman, A. H.; Brauman, J. I. J. Chem. Phys. **1979**, 71, 2088. (e) Jackson, R. L.; Pellerite, M. J.; Brauman, J. I. J. Am. Chem. Soc. **1981**, 103, 1802. (f) Jackson, R. L.; Pellerite, M. J.; Brauman, J. I. J. Phys. Chem. **1981**, 85, 1624. (g) Draic, P. S. Brauman, J. I. J. Phys. Chem. **1984**, 88, 5285. (h) Janousek, B. K.; Zimmerman, A. H.; Reed, K. J.; Brauman, J. I. J. Am. Chem. Soc. **1978**, 100, 6142. (i) Janousek, B. K.; Reed, K. J.; Brauman, J. I. J. Am. Chem. Soc. **1980**, 102, 3125. (j) Moylan, C. R.; Dodd, J. A.; Brauman, J. I. Chem. Phys. Lett. **1985**, 118, 38. (k) Drzaic, P. S.; Brauman, J. I. J. Am. Chem. Soc. **1982**, 104, 13. (l) Keingeld, J. C.; Ingemann, S.; Jolonen, J. E.; Nibbering, N. M. M. J. Am. Chem. Soc. **1983**, 105, 2474.

28. (a) Jackson, R. L.; Hiberty, P. C.; Brauman, J. I. Chem. Phys. **1981**, 74, 3605. (b) Lykke, K. R.; Mead, R. D.; Lineberger, W. C. Phys. Rev. Lett. **1984**, 52, 2221. (c) Marks, J.; Wtzel, D. M.; Comita, P. B.; Brauman, J. I. J. Chem. Phys. **1986**, 84, 5284. (d) Mead, R. D.; Lykke, K. R.; Lineburger, W. C.; Marks, J.; Brauman, J. I. Chem. Phys. **1984**, 81, 4883.

29. (a) Mosely, J. T.; Cosby, P. C.; Bennett, R. A.; Peterson, J. R. J. Chem. Phys. **1975**, 62, 4826 and references therein.

(b) Mosely, J. T.; Cosby, P. C.; Ling,J. H.; Peterson, J. R. J. Chem. Phys. **1977**, 65, 5267. (c) Hodges, R. V.; Lee, L. C.; Moseley. J. T. J. Chem. Phys. **1980**, 72, 2998. (d) Mosely, J. T.; Cosby, P. C.; Lee, L. C.; Peterson, J. R.; Smith, G. P. J. Chem. Phys. **1978**, 68, 3818. (e) Mosely, J. T.; Cosby, P. C.; Smith, G. P. J. Chem. Phys. **1978**, 69, 2779. (f) Mosely, J. T.; Cosby, P. C.; Huber, B. A.; Peterson, J. R. J. Chem. Phys. **1977**, 66, 4520. (g) Mosely, J. T.; Cosby, P. C.; Peterson, J. R. J. Chem. Phys. **1976**, 65, 2512. (h) Mosely, J. T.; Cosby, P. C.; Smith, G. P. J. Chem. Phys. **1977**, 67, 3818. (i) Mosely, J. T.; Lee, L. C.; Smith, G. P. J. Chem. Phys. **1979**, 71, 4034. (j) Mosely, J. T.; Cosby, P. C.; Bennett, R. A.; Peterson, J. R. J. Chem. Phys. **1975**, 63, 1612. (k) Mosely, J. T.; Cosby, P. C.; Lee, L. C.; Peterson, J. R.; Smith, G. P.; Guest, J. A. J. Chem. Phys. **1979**, 70, 3237.

30. Cosby, P. C.; Ling, J. H.; Peterson, J. R.; Moseley, J. T. J. Chem. Phys. **1976**, 12, 5267.

31. Ferguson, E. E.; Fehnsenfeld, F. C.; Phelps, A. V. J. Chem. Phys., **1973**, 59, 1565.

32. Hotop, H.; Lineberger, W. C. J. Phys. Chem. Ref. Data. **1975**, 4, 539.

33. Hong, S. P.; Woo, S. B.; Helmy, E. M. Bull. Am. Phys. **1976**, 21, 170.

34. (a) Maguire, T. C.; Brooks, P. R.; Curl, R. F.; Spence J. H.; Ulvick, S. J. J. Chem. Phys. **1986**, 85, 844.

35. (a) Brauman, J.I.; Stephenson, L.M.; Richardson, J.H. J. Am. Chem. Soc., **1974**, 96, 3671.

36. Geltman, S. Phys. Rev. **1958**, 112, 176.

37. Burch, D. S.; Smith, S. J.; Branscomb, L. M. Phys. Rev. **1958**, 112, 171.

38. Proctor, A.; Sherwood, P. M. A. Anal. Chem. **1982**, 54, 13.

39. Proctor, A.; Sherwood, P. M. A. Anal. Chem. **1980**, 52, 2315.

40. Personal communication with W. C. Lineberger.

41. Bartmass, J. E. J. Am. Chem. Soc. **1980**, 102, 2483

42. Fukuda, E. K.; McIver, R. T. J. Am. Chem. Soc. **1979**, 101, 2498.

43. Hartung, W. H.; Crossley, F. Org. Synth. Coll. Vol. II, **1943**, 363.

44. Doering, W. von E. DePuy, C. H. J. Am. Chem. Soc. **1953**, 75, 5955.

45. I thank Daniel J. Reed for the preparation of diazocyclopentadiene.

46. This explosion occured after the diazo compound had been collected. As the undistilled material remaining in the flask was allowed to come to 760 torr the explosion occured. The explosion was large enough to break the exhaust hoods blast glass and damage the exhaust hood.

47. Domenico, A. di; Harland, P.W.; Franklin, J.L. J. Chem Phys. **1972**, 56, 5299.

48. $\underline{c}\text{-}C_5H_5^-$ + $(CF_3)_2CHOH \rightarrow \underline{c}\text{-}C_5H_6$ + $(CF_3)_2CHO^-$, k_{total} = 1.3 x 10^{-9} cm^3 $molecule^{-1}$ sec^{-1}; $\underline{c}\text{-}C_5H_5^-$ + $CF_3CH_2OH \rightarrow \underline{c}\text{-}C_5H_6$ + $CF_3CH_2O^-$, k_{total} = 3.1 x 10^{-10} cm^3 $molecule^{-1}$ sec^{-1}.

49. Zimmerman, A. H.; Brauman, J. I. J. Chem. Phys. **1977**, 66, 5823

50. Jackson, R. J.; Zimmerman, A. H.; Brauman, J. I. J. Chem. Phys. **1979**, 71, 2088

51. Lineberger, W. C.; Engleking, P. C. J. Chem Phys. **1977**, 1412.

52. Kiss, A. I.; Horvath, G. Acta. Chim. **1970**, 66, 431

53. Levy, J.; Leblond, M. Phys. Rev. **1967**, 153, 1.

54. Sherwood, P. M. A. Briggs, D.; Seah, M. P.; Ed. "Pactical Surface Analysis by Auger and X-ray Photoelectron Spectroscopy."; John Wiley & Sons, 1983

55. Turner, J. E.; Anderson, V. E.; Fox, K. Phys. Rev. **1968**, 174, 81.

56. Turner, J. E.; Fox, K. Phys. Lett. **1966**, 91, 547.

57. Brauman, J. I. ; Richardson, J. H.; Stephson, L. M. J. Am. Chem. Soc. **1975**, 97, 2967.

58. Wendoloski, J. J.; Jordan, K. D. Mol. Phys. **1978**, 35, 223.

59. Rohr, K.; Lindler, F. J. Phys. **1976**, B 9, 2521.

60. Wong, S. F.; Schultz, G. J. Phys. Rev. Lett. **1974**, 33, 134.

61. Dude, L.; Hezenberg, J. J. Phys. Rev. Lett. **1977**, 21, 145

62. Nelson, R. D., Jr.; Lide, D. R.; Maryott, A. A. "Selected Values of Electric Dipole Moments for Molecules in the Gas Phase." NSRDS-NBS10, U.S. Government Printing Office, Washington, D.C, 1967.

63. (a) Jackson, R. L.; Hiberty, P. C.; Brauman, J. I. J. Chem. Phys. **1981**, 74, 3705. (b) Lykke, K. R.; Mead, R. D.; Lineberger, W. C.

Phys. Rev. Lett. **1984**, 52, 2221. (c) Lykke, K. R.; Mead, R. D.; Lineberger, W. C. J. Chem. Phys. **1984**, 81, 4883.

64. Engelking, P. C.; Lineberger, W. C. J. Chem. Phys. **1977**, 67, 1412.
65. Hedaya, E. Acc. Chem Res. **1969**, 2, 367.
66. Leibling, G. R.; McConnell, H. M. J. Chem. Phys. **1965**, 2, 3931.
67. Purins, D.; Feeley, H. F. J. Mol. Struct. **1974**, 22, 11.
68. Heydaya, E. "High Temperature Reactions by Flash Vacuum Pyrolsis," in **IUPAC, XXIII International Congress** Butterworths, London, **1971**, 4, 195.
69. I thank Dr. Cheng Tung for the determination of EPD spectrum of c-$C_5H_5^-$.
70. Sado, A.; West, H. P.; Schafer, L. Spectrochim. Acta. **1966**, 22, 11.
71. Fritx, H. P.; Schafer, L. Chem. Ber. **1964**, 97, 1829.
72. Janousek, B. K.; Zimmerman, A. H.; Reed, K. J.; Brauman, J. I. J. Am. Chem. Soc. **1978**, 100, 6142.
73. Janousek, B. K.; Reed, K. J.; Brauman, J. I. J. Am. Chem. Soc. **1980**, 102, 3125.
74. Bofill, J. M.; Bru, N.; Farràs, J.; Olivella, S.; Solé, A.; Villarrasa, J. J.Am. Chem. Soc. **1988**, 110, 3740.
75. Wasserman, E.; Barash, L.; Trozzolo, J.; Murray, R. W.; Yager, W. A. J. Am. Chem. Soc. **1964**, 86, 2304.
76. The original repoert of the PA(c-$C_5H_4^{\bullet -}$) was in error due to an error in the determination of the PA of the bracketing reagents. The value reported is the corrected value.

77. "JANAF Thermochemical Tables", Natl. Stand. Ref. Data Ser., Natl. Bur. Stand. **1971**, No. 37.

78. Furuyama, S.; Golden, D. M.; Benson, S. W. Int. J. Chem. Kinet. **1971**, 3, 237.

79. J. Phys. Chem. Ref. Data 1982, 11, 38.

80. Stull, D. R.; Westrum, E. F.; Sinke G. C. "The Chemical Thermodynamics of Organic Compounds" Wiley, New York, 1969, pg. 367

81. J. Chem. Phys. Ref. Data **1977**, 6, 70.

82. McDonald, R. N.; Chowdury, A. K.; Schell, P. L. J. Am. Chem. Soc. **1984**, 106, 6095.

83. McDonald R. N.; Schell, P. L. Organometallics **1988**, 7, 1820.

84. Weast, R. C. "CRC Handbook of Chemistry and Physics", 64th ed., CRC Press, Boca Raton, Florida, 1983.

85. Guenzburger, D.; Saitovitch, E. M.; De Paoli, M. A.; Manela, H. J. Chem. Phys. **1984**, 80, 735.

86. Breeze, P. A.; Burdett, J. K.; Turner, J. J. Inorg. Chem. **1981**, 20, 3369.

87. Su. T.; Bowers, M.T. J. Chem. Phys. **1973**, 58, 3027.

88. Castellan, G. W. "Physical Chemistry" 2nd ed., Addison-Wesley, Reading, Mass., 1971, p. 626.

89. Laidler, K. J. In "Chemical Kinetics" Harper & Row, New York, 3rd Ed., 1987, Chap. 4.

Acknowledgement.

First, I would like to thank my advisor, Professor Richard McDonald, for his patience and guidance. I am most grateful to Dr. Roger Beaman for the help in the early stages of this investigation. The data aquisition system is the result of great efforts on the part of Mark Matson and John Linzi. My thanks also go to Daniel Reed for his help in classes and numerous discussions. I would also like to thank Dr. Cheng Tung for the determination of the EPD spectrum of c-$C_5H_4^-$ and Gerry Greb for disscusions concerning the experiment.

This research would not have been possible without the support from National Science Foundation.

I would like to thank my wife, Jennifer, for her support, confidence, and help in the decision to attend graduate school. I also need to acknowledge the confidence of my Mother and Father who never gave up on their son. It is through their support and guidance, along with that of my wife, that has truly made this work possible.

Laser Induced Electron Photodetachment in a Flowing Afterglow

by

Edward John Bianchina, Jr.

B.S., Northwest Missouri State University, 1986

AN ABSTRACT OF A MASTER'S THESIS

submitted in partial fulfillment of the

requirements for the degree

MASTER OF SCIENCE

Department of Chemistry

KANSAS STATE UNIVERSITY

Manhattan, Kansas

1989

Abstract.

A method for the determination of high resolution relative electron photodetachment (EPD) spectra for negative ions was developed. The negative ions which were generated in a flowing afterglow (FA) were crossed with laser beam. The photon beam was generated by a tunable dye laser operated in an extended cavity mode, which was constructed by removing the normal output coupler of the laser and placing a highly reflective mirror on the far side of the FA main housing so as to incorporate a cross section of the FA within the extended laser cavity.

Because the EPD spectra had not been previously determined in a FA, the EPD spectrum for acetophenone enolate anion ($C_6H_5C(O^-)=CH_2$) was determined to verify the resolution of the FA/laser system; the EPD spectum of this anion had been previously determined using an ion cyclotron resonance spectrometer/laser system. To verify the accuracy of EPD threshold determinations, the EPD spectrum of cyclopentadienyl anion ($\underline{c}$-$C_5H_5^-$) was determined. The EA($\underline{c}$-$C_5H_5\bullet$) had been established by photoelectron spectroscopy (PES) to be 1.786 ± 0.020 eV. By fitting the FA/laser EPD spectrum to a threshold law, EA($\underline{c}$-$C_5H_5\bullet$) = 1.753 ± 0.007 eV was determined.

The objective of this study was to determine the EPD spectrum of cyclopentadienylidene anion radical ($\underline{c}$-$C_5H_4^{\bullet -}$). The threshold of the EPD spectrum of $\underline{c}$-$C_5H_4^{\bullet -}$(708 ± 3 nm) yielded EA($\underline{c}$-$C_5H_4(^3B_1)$) = 40.37 ± 0.16 kcal mol^{-1}. Several plateaus were observed and assigned to the

onset of the EPD thresholds of three electronic excited state of the carbene $\underline{c}$-C_5H_4 ; $^1A_2$ = 5.83 ± 0.15 (619 ± 3 nm), $^3A_2$ = 7.43 ± 0.15 (598 ± 3 nm), and $^1A'$ = 9.23 ± 0.15 (576 ± 3 nm) kcal mol^{-1} above the $^3B_1$ ground state. These values agree reasonably with the calculated $\delta\Delta\underline{H}^\circ_f$ values for these three states. This data and $\Delta\underline{H}^\circ_{f,298}(\underline{c}\text{-}C_5H_4^{\bullet -})$ = 71.6 ± 3.2 kcal mol^{-1} allows for the calculation of the heats of formation of the various states of $\underline{c}$-C_5H_4; $\underline{c}$-$C_5H_4(^3B_1)$ $\Delta\underline{H}^\circ_{f,298}$ = 111.97 ± 3.4 kcal mol^{-1}, excited states, $\Delta\underline{H}^\circ_{f,298}(\underline{c}\text{-}C_5H_4(^1A_2))$ = 117.74 ± 3.4 , $\Delta\underline{H}^\circ_{f,298}(\underline{c}\text{-}C_5H_4(^3A_2))$ = 119.37 ± 3.4, and $\Delta\underline{H}^\circ_{f,298}(\underline{c}\text{-}C_5H_4(^1A'))$ = 121.23 ± 3.4 kcal mol^{-1}.